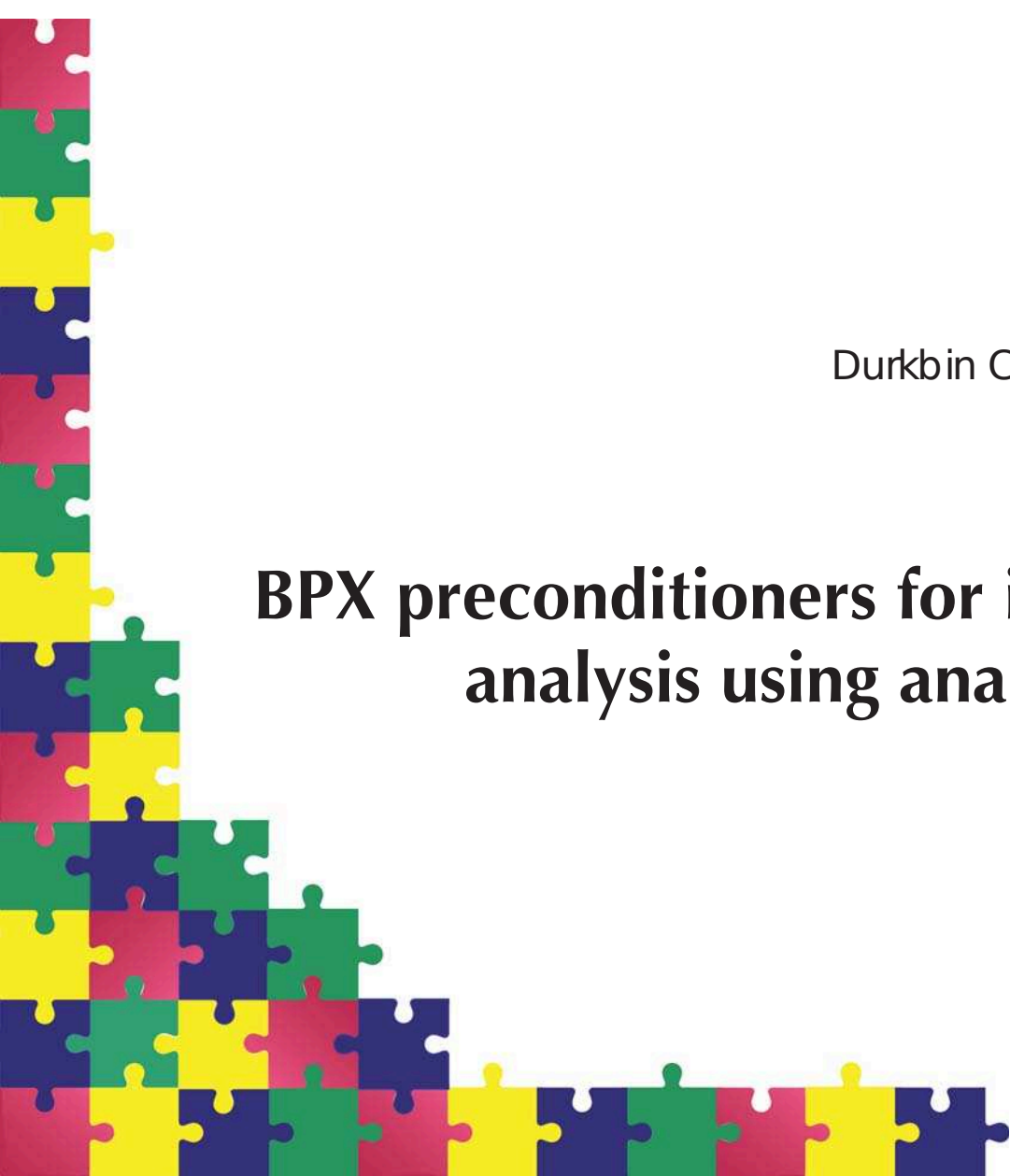# imati

REPORT SERIES

Durkbin Cho, Rafael Vázquez

BPX preconditioners for isogeometric analysis using analysis-suitable T-splines

IMATI REPORT Series

Nr. 17-01– January 2017

Managing Editor

Paola Pietra

Editorial Office

Follow this and additional works at: http://www.imati.cnr.it/reports

BPX preconditioners for isogeometric analysis using analysis-suitable T-splines

D. Cho, R. Vázquez

Durkbin Cho:
Department of Mathematics, Dongguk University, Pil-dong 3-ga, Jung-gu, Seoul, 100-715, South Korea.
E-mail address: durkbin@dongguk.edu

Rafael Vázquez:
Istituto di Matematica Applicata e Tecnologie Informatiche `E. Magenes' del CNR, via Ferrata 5, 27100, Pavia, Italy.
E-mail address: vazquez@imati.cnr.it

_____

Abstract.

We propose and analyze optimal additive multilevel solvers for isogeometric discretizations of scalar elliptic problems for locally refined T-meshes. Applying the refinement strategy in [32] we can guarantee that the obtained T-meshes are **p**-admissible, which implies that the associated T-splines are analysis suitable. Taking advantage of the multilevel structure of **p**-admissible T-meshes, we develop a BPX preconditioner on the basis of local smoothing only for the functions affected by a newly added edge by bisection, and prove that our method has optimal complexity. Several numerical experiments confirm our theoretical result and also show the practical performance of the proposed preconditioner.

[page left intentionally blank]

BPX preconditioners for isogeometric analysis using analysis-suitable T-splines

Durkbin Cho[*]   Rafael Vázquez[†]

Abstract

We propose and analyze optimal additive multilevel solvers for isogeometric discretizations of scalar elliptic problems for locally refined T-meshes. Applying the refinement strategy in [32] we can guarantee that the obtained T-meshes are **p**-admissible, which implies that the associated T-splines are analysis suitable. Taking advantage of the multilevel structure of **p**-admissible T-meshes, we develop a BPX preconditioner on the basis of local smoothing only for the functions affected by a newly added edge by bisection, and prove that our method has optimal complexity. Several numerical experiments confirm our theoretical result and also show the practical performance of the proposed preconditioner.

1   Introduction

The analysis and development of adaptive schemes is one of the most active areas of research in the context of isogeometric analysis (IGA), a recent methodology for the solution of partial differential equations with high continuity splines. The main idea of adaptive methods is to obtain a good accuracy of the solution with less computational effort by applying local mesh refinement, hence adaptive IGA schemes require the use of different spline spaces that break the tensor-product structure of B-splines. The most popular alternatives in the IGA research community are T-splines [36], LR-splines [19, 28] and hierarchical splines [38].

In particular, in this paper we focus on T-splines, introduced by Sederberg et al. in [36] and applied in IGA for the first time in [2, 22]. T-splines are constructed from a T-mesh, a rectangular tiling with hanging nodes, and T-spline blending functions are defined from their local knot vectors, which are computed from the tiling. The mathematical research on T-splines has been very active in recent years, and it has led to the introduction of analysis-suitable (or dual compatible) T-splines [31, 4, 5, 30], a subset of T-splines with good approximation properties that provide local linear independence.

A standard adaptive scheme based on mesh refinement can be written in a loop of the form [15]

$$\textbf{SOLVE} \longrightarrow \textbf{ESTIMATE} \longrightarrow \textbf{MARK} \longrightarrow \textbf{REFINE},$$

and suitable strategies for all the steps of the adaptive scheme are needed in order to guarantee its efficiency. Numerical tests show that traditional a posteriori estimators and marking strategies from finite elements can be adapted to IGA with good results, see for instance [22] and [13]. Local

---

[*]Department of Mathematics, Dongguk University, Pil-dong 3-ga, Jung-gu, Seoul, 100-715, South Korea.
E-mail address: `durkbin@dongguk.edu`

[†]Istituto di Matematica Applicata e Tecnologie Informatiche 'E. Magenes' del CNR, via Ferrata 1, 27100, Pavia, Italy.
E-mail address: `vazquez@imati.cnr.it`

refinement strategies for T-splines were first studied in [35], but up to our knowledge the only local refinement strategy that has been proved to be optimal is the one in [32], which is based on refining elements by bisection, alternating the refinement direction.

In this paper we focus on the solution of the linear system arising in the **SOLVE** module for T-splines, and study the optimality of a suitable BPX preconditioner. Several domain decomposition preconditioners have been recently studied in the IGA context: overlapping Schwarz methods [8], balancing domain decomposition by constraint (BDDC) methods [7, 3] and dual primal isogeometric tearing and interconnecting methods [29, 33]. Multilevel preconditioners for IGA have been extensively analyzed in the tensor-product setting: the BPX preconditioner in [14], and multigrid preconditioners [23, 25, 26, 24, 21].

The T-splines obtained with the refinement strategy in [32] are analysis-suitable by construction, and present a multilevel structure, which makes them very appealing to apply multilevel preconditioners. In the present paper, we first present theoretically optimal multilevel preconditioners for IGA on *locally refined* T-meshes, extending the results in [14] to T-splines.

For the study of the optimality of the BPX preconditioner we follow [15], writing the preconditioner in the framework of the parallel subspace correction (PSC) method. In this framework, the optimality follows from two basic properties: a stable space decomposition, and the strengthened Cauchy-Schwarz inequality. The proof of these two properties is the core of this work, and as a consequence we obtain that the BPX preconditioner gives a uniformly bounded condition number, which is independent of the mesh size h, but depends on the degree p as in [14].

The construction of the BPX preconditioner as in [15] is performed by adding a new edge to the T-mesh by bisection, and the new level is defined by the functions appearing or modified by the insertion of this edge. An alternative construction is also proposed, adding all the edges of the same generation at once, and defining the functions of the new level as those appearing or modified after the insertion of all edges. The theoretical optimality for this alternative construction, that we name *macro* decomposition, follows from the previous one, but the numerical results show an improved performance.

The paper is organized as follows. In Section 2, we introduce the framework of parallel subspace correction (PSC) method and present its convergence theory based on the two properties mentioned above. We briefly review the basics of univariate/multivariate B-splines in Section 3. In Section 4, we give a new definition of T-meshes by bisections and discuss **p**-admissible T-meshes and their fundamental properties as in [32]. In Section 5, we construct a space decomposition on **p**-admissible T-meshes and then prove that the two aforementioned properties are satisfied. In Section 6 we obtain the optimality result for the BPX preconditioner, and also deal with the macro decomposition, showing that is also an efficient space decomposition for the purpose of implementation. Some numerical results that validate our theory are presented in Section 7.

2 Preliminaries

2.1 Problem setting

We are interested in the second order Laplacian with homogeneous Dirichlet boundary conditions,

$$-\Delta u = f \quad \text{in} \ \ \Omega, \qquad u = 0 \quad \text{on} \ \ \partial\Omega, \tag{1}$$

where $\partial\Omega$ denotes the boundary of Ω and $f \in L^2(\Omega)$. The isogeometric approximation to the solution of (1) is the function $u \in \mathcal{V}$ such that

$$a(u, v) = (f, v) \quad \forall v \in \mathcal{V}$$

where

$$a(u, v) = \int_\Omega \nabla u \cdot \nabla v \ dx, \quad (f, v) = \int_\Omega fv \ dx,$$

and $\mathcal{V}$ is the isogeometric discrete space. Defining a linear operator $A : \mathcal{V} \to \mathcal{V}$ by

$$(Au, v) = a(u, v), \ \forall u, v \in \mathcal{V}$$

and also $b \in \mathcal{V}$ by $(b, v) = (f, v), \ \forall v \in \mathcal{V}$, we have to solve the linear operator equation

$$Au = b$$

for some $u \in \mathcal{V}$.

In the rest of the paper, we will adopt the following compact notation. Given two real numbers a, b we write $a \lesssim b$, when $a \leq Cb$ for a generic constant C independent of the knot vectors (defined below), and we write $a \approx b$ when $a \lesssim b$ and $b \lesssim a$.

2.2 Iterative methods

Iterative schemes for the solution of $Au = b$ can be written in the form

$$u^{k+1} = u^k + B(b - Au^k), \quad k = 0, 1, 2, \ldots, \tag{2}$$

starting from an initial guess $u^0 \in \mathcal{V}$. The core of the iterative methods is the iteration matrix B, which is an approximate of the inverse of A. In case of being symmetric positive definite (SPD), the iteration matrix B can be used as a preconditioner of A for iterative methods. The preconditioned conjugate gradient (PCG) method can be understood as a conjugate gradient method applied to the preconditioned system

$$BAu = Bb,$$

Let $u^k, \ k = 0, 1, 2, \ldots$, be the solution sequence of the PCG algorithm. Then the following error estimate is well-known:

$$\|u - u^k\|_A \leq 2 \left(\frac{\sqrt{\kappa(BA)} - 1}{\sqrt{\kappa(BA)} + 1} \right)^k \|u - u^0\|_A,$$

which implies that the PCG method converges faster with a smaller condition number $\kappa(BA)$.

2.3 The method of parallel subspace corrections

The method of parallel subspace corrections (PSC) provides a particular construction of the itaration matrix B. The starting point is a suitable decomposition of $\mathcal{V}$:

$$\mathcal{V} = \sum_{i=0}^J \mathcal{V}_i,$$

where $\mathcal{V}_i$ are subspaces of $\mathcal{V}$. The model problem (1) can be split into sub-problems in each $\mathcal{V}_i$ with smaller size. Throughout this paper, we use the following operators, for $i = 0, 1, \ldots, J$:

- $Q_i : \mathcal{V} \to \mathcal{V}_i$ the projection in the inner product $(\cdot, \cdot)$;

- $I_i : \mathcal{V}_i \to \mathcal{V}$ the natural inclusion;

- $A_i : \mathcal{V}_i \to \mathcal{V}_i$ the restriction of A to the subspace $\mathcal{V}_i$;

- $R_i : \mathcal{V}_i \to \mathcal{V}_i$ an approximation of A_i^{-1}.

This method performs the correction on each subspace in parallel. In operator form, it reads like (2) with the iteration matrix defined by

$$B := \sum_{i=0}^{J} I_i R_i I_i^t \quad \Big(= \sum_{i=0}^{J} R_i Q_i \Big). \tag{3}$$

The corresponding error equation reads

$$u - u^{k+1} = \Big[I - \Big(\sum_{i=0}^{J} I_i R_i I_i^t \Big) A \Big] (u - u^k).$$

The convergence analysis of (PSC) is based on the following two important properties [15]:
(A1) Stable Decomposition For any $v \in \mathcal{V}$, there exists a decomposition $v = \sum_{i=0}^{J} v_i$, $v_i \in \mathcal{V}_i$, $i = 0, \ldots, J$ such that

$$\sum_{i=0}^{J} \|v_i\|_A^2 \le K_1 \|v\|_A^2.$$

(A2) Strengthened Cauchy-Schwarz (SCS) inequality For any $u_i, v_i \in \mathcal{V}_i, i = 0, \ldots, J$

$$\left| \sum_{i=0}^{J} \sum_{j=i+1}^{J} (u_i, v_j)_A \right| \le K_2 \left(\sum_{i=0}^{J} \|u_i\|_A^2 \right)^{1/2} \left(\sum_{i=0}^{J} \|v_i\|_A^2 \right)^{1/2}.$$

For a space decomposition satisfying both properties, one can prove the following result on the preconditioned linear system [15]:

Theorem 2.1 *Let* $\mathcal{V} = \sum_{i=0}^{J} \mathcal{V}_i$ *be a space decomposition satisfying* **(A1)** *and* **(A2)**, *and let* R_i *be SPDs for* $i = 0, \ldots, J$ *such that*

$$K_4^{-1} \|u_i\|_A^2 \le (R_i^{-1} u_i, u_i) \le K_3 \|u_i\|_A^2. \tag{4}$$

Then B *defined by* (3) *is SPD and*

$$\kappa(BA) \le (1 + 2K_2) K_1 K_3 K_4. \tag{5}$$

The goal of the paper is the construction of a preconditioner like (3) for T-splines, and the proof that **(A1)** and **(A2)** are satisfied.

3 Splines

In this section we recall the definition and main properties of B-splines, mainly to fix the notation. For a more extensive description on the use of splines in isogeometric analysis, the reader is referred to [27, 16], and to [6] for a mathematical perspective.

3.1 Univariate B-splines

Given two positive integers p and n, we say that $\Xi := \xi_0, \ldots, \xi_{n+p}$ is a p-open knot vector if

$$0 = \xi_0 = \cdots = \xi_p < \xi_{p+1} \leq \cdots \leq \xi_{n-1} < \xi_n = \cdots = \xi_{n+p} = 1,$$

where repeated knots are allowed. From the knot vector Ξ, univariate B-spline basis functions of degree p are defined recursively using the Cox-De Boor formula (see [17]). The definition of each B-spline $B_{i,p}$, $i = 0, \ldots, n-1$, is determined by a $p+2$ local knot vector $\Xi_{i,p} = \{\xi_i, \ldots, \xi_{i+p+1}\}$. Whenever necessary, we will stress it by adopting the following notation:

$$B_{i,p}(\zeta) = B[\Xi_{i,p}](\zeta), \quad \zeta \in (0,1).$$

Thus, the basis function $B_{i,p}$ has support

$$\operatorname{supp}(B_{i,p}) = [\xi_i, \xi_{i+p+1}].$$

Let us select from Ξ a subset $\{\xi_{i_k}, k = 0, \ldots, N\}$ of non-repeated knots, or breakpoints, with $\xi_{i_0} = 0$, $\xi_{i_N} = 1$. We point out that the local mesh size of the element $I_k = (\xi_{i_k}, \xi_{i_{k+1}})$ is called $h_k = \xi_{i_{k+1}} - \xi_{i_k}$ for $k = 0, \ldots, N-1$. Moreover, to the element $I_k = (\xi_{i_k}, \xi_{i_{k+1}})$, that can be written as (ξ_j, ξ_{j+1}) for a certain j, we associate the *support extension* $\widetilde{I}_j$ defined by

$$\widetilde{I}_j := (\xi_{j-p}, \xi_{j+p+1}). \tag{6}$$

We denote by

$$\mathcal{S}_p(\Xi) := \operatorname{span}\{B_{i,p}, i = 0, \ldots, n-1\}.$$

the univariate B-splines space spanned by those B-splines of degree p. The functions $B_{i,p}$ are a *partition of unity*, as shown in [34].

Following [34, Theorem 4.41], we define suitable functionals $\lambda_{j,p} = \lambda[\xi_j, \ldots, \xi_{j+p+1}]$, for $0 \leq j \leq n-1$, which are dual to the B-splines basis functions, that is

$$\lambda_{j,p}(B_{i,p}) = \delta_{ij}, \qquad 0 \leq i, j \leq n-1,$$

where δ_{ij} is the Kronecker delta. The following estimate of the functionals $\lambda_{j,p}$ will be useful in the sequel.

Lemma 3.1 *If $f \in L^q(\xi_j, \xi_{j+p+1})$, with $1 \leq q \leq +\infty$ then*

$$|\lambda_{j,p}(f)| \lesssim |\xi_{j+p+1} - \xi_j|^{-1/q} \|f\|_{L^q(\xi_j, \xi_{j+p+1})}.$$

Proof. The proof can be found in [34, Theorem 4.41]. $\qquad\square$

We note that these dual functionals are locally defined and depend only on the corresponding local knot vector, namely,

$$\lambda_{i,p}(f) = \lambda[\Xi_{i,p}](f).$$

Let $\Pi_{p,\Xi}$ be the projection that is built from the dual basis as detailed in [34, Theorem 12.6], that is,

$$\Pi_{p,\Xi} : L^2([0,1]) \to \mathcal{S}_p(\Xi), \qquad \Pi_{p,\Xi}(f) = \sum_{j=0}^{n-1} \lambda_{j,p}(f) B_{j,p}. \tag{7}$$

Assumption 3.1 $\{\xi_{i_0}, \xi_{i_1}, \ldots, \xi_{i_N}\}$ *is locally quasi-uniform, that is, there exists a constant $\theta \geq 1$ such that the mesh sizes $h_k = \xi_{i_{k+1}} - \xi_{i_k}$ satisfy the relation $\theta^{-1} \leq h_k/h_{k+1} \leq \theta$, for $k = 0, \ldots, N-2$.*

Proposition 3.2 *For any non-empty knot span $I_k = (\xi_{i_k}, \xi_{i_{k+1}})$, we have*

$$\|\Pi_{p,\Xi}(f)\|_{L^2(I_k)} \leq C\|f\|_{L^2(\widetilde{I}_k)},$$

where the constant C depends only on the degree p. Moreover, if Assumption 3.1 holds, we have

$$|\Pi_{p,\Xi}(f)|_{H^1(I_k)} \leq C|f|_{H^1(\widetilde{I}_k)},$$

where the constant C depends only on p and θ and H^1 denotes the classical Sobolev norm.

Proof. The proof can be found in [6, Proposition 2.2]. □

3.2 Multivariate splines

Multivariate B-splines can be constructed by means of tensor products. We discuss here the bivariate case, the higher-dimensional case being analogous.

For $d = 1, 2$, assume that $n_d \in \mathbb{N}$, the degree p_d and the p_d-open knot vector $\Xi_d = \{\xi_{d,0}, \dots, \xi_{d,n_d+p_d}\}$ are given. We set the polynomial degree vector $\mathbf{p} = (p_1, p_2)$ and $\Xi = \{\Xi_1, \Xi_2\}$. We introduce a set of multi-indices $\mathbf{I} = \{\mathbf{i} = (i_1, i_2) : 0 \leq i_d \leq n_d - 1\}$ and for each multi-index $\mathbf{i} = (i_1, i_2)$, we define the local knot vector

$$\Xi_{\mathbf{i},\mathbf{p}} = \{\Xi_{i_1,p_1}, \Xi_{i_2,p_2}\}.$$

Then we can introduce the set of multivariate B-splines

$$\{B_{\mathbf{i},\mathbf{p}}(\boldsymbol{\zeta}) = B[\Xi_{i_1,p_1}](\zeta_1)B[\Xi_{i_2,p_2}](\zeta_2), \quad \text{for all } \mathbf{i} \in \mathbf{I}\}.$$

The spline space in the parametric domain $\Omega = (0,1)^2$ is then

$$S_{\mathbf{p}}(\Xi) = \text{span}\{B_{\mathbf{i},\mathbf{p}}(\boldsymbol{\zeta}), \quad \mathbf{i} \in \mathbf{I}\}.$$

We also introduce the set of non-repeated interface knots for each direction $\{\xi_{d,i_0}, \dots, \xi_{d,i_{N_d}}\}$, $d = 1, 2$, which determine the intervals $I_{d,j_d} = (\xi_{d,i_{j_d}}, \xi_{d,i_{j_d+1}})$, for $0 \leq j_d \leq N_d - 1$. These intervals lead to the Cartesian grid $\mathcal{M}^{\mathcal{B}}$ (or simply $\mathcal{M}$) in the unit domain $\Omega = (0,1)^2$, also called the Bézier mesh:

$$\mathcal{M}^{\mathcal{B}} = \{Q_{\mathbf{j}} = I_{1,j_1} \times I_{2,j_2}, \text{ for } 0 \leq j_d \leq N_d - 1\}.$$

For a generic element $Q_{\mathbf{j}}$, we also define its support extension

$$\widetilde{Q}_{\mathbf{j}} = \widetilde{I}_{1,j_1} \times \widetilde{I}_{2,j_2},$$

with $\widetilde{I}_{d,j_d}$ the univariate support extension by (6).

3.2.1 Multivariate quasi-interpolants

We note that when the univariate quasi-interpolants are defined from a dual basis, as in (7), then the multivariate quasi-interpolant is also defined from a dual basis. Indeed, we have

$$\Pi_{\mathbf{p},\Xi}(f) = \sum_{\mathbf{i}\in\mathbf{I}} \lambda_{\mathbf{i},\mathbf{p}}(f)B_{\mathbf{i},\mathbf{p}}, \tag{8}$$

where each dual functional is defined from the univariate dual bases by the expression

$$\lambda_{\mathbf{i},\mathbf{p}} = \lambda_{i_1,p_1} \otimes \lambda_{i_2,p_2}.$$

6

4 T-splines

The main drawback of B-splines is their tensor-product structure, which prevents local refinement as required by adaptive methods. One of the alternatives is the use of T-splines [36], a superset of B-splines that allows for local refinement. The use of T-splines in IGA was first explored in [2, 22], and it has led to a growing interest for the analysis of their mathematical properties. In this section we are collecting mathematical results from [31, 4, 5] (linear-independence, dual basis and projectors), [30, 12] (nestedness and space characterization) and [6, Section 7] (local linear independence), following mainly the notation in [6].

We restrict ourselves to T-splines where refinement is always performed by bisection, and the multiplicity is never reduced. A more general setting can be considered, but it would only add technical difficulties without adding more insight.

4.1 T-mesh defined by bisection

As in the previous section, let us assume that we are given the degrees p_d, the integers n_d and the open knot vectors Ξ_d, and let us denote $m_d = n_d + p_d$ for $d = 1, 2$. For simplicity we assume that the internal knots in Ξ_d are not repeated and *equally spaced*, so the element size in each parametric direction can be denoted by h_1 and h_2. Our starting point is the index mesh $\mathcal{T}_0$ in the index domain $[0, m_1] \times [0, m_2]$, defined as the Cartesian grid of unit squares

$$\mathcal{T}_0 = \{[j_1, j_1 + 1] \times [j_2, j_2 + 1] : j_1 = 0, \ldots, m_1 - 1; \; j_2 = 0, \ldots, m_2 - 1\},$$

which is associated to the tensor-product B-spline space $S_{\mathbf{p}}(\mathbf{\Xi})$.

To define T-splines by bisection, we start introducing, for any integer $\ell \geq 0$ and for $d = 1, 2$, the set of rational indices

$$\mathcal{I}_d^\ell = \left\{0, \ldots, p_d, p_d + \frac{1}{2^\ell}, \ldots, p_d + \frac{2^\ell - 1}{2^\ell}, p_d + 1, \ldots, n_d - 1, n_d - 1 + \frac{1}{2^\ell}, \ldots, n_d - 1 + \frac{2^\ell - 1}{2^\ell}, n_d, n_d + 1, \ldots, n_d + p_d\right\},$$

and we notice that $\mathcal{I}_d^\ell \subset \mathcal{I}_d^{\ell'}$ if $\ell \leq \ell'$. We also define the ordered knot vectors

$$\Xi_d^\ell = \{\xi_{d,k}, \; k \in \mathcal{I}_d^\ell\} = \left\{\xi_{d,0}, \xi_{d,1}, \ldots, \xi_{d,p_d}, \xi_{d,p_d + \frac{1}{2^\ell}}, \ldots, \xi_{d,n_d - 1 + \frac{2^\ell - 1}{2^\ell}}, \xi_{d,n_d}, \xi_{d,n_d + 1}, \ldots, \xi_{d,n_d + p_d}\right\},$$

in a recursive way: starting from $\Xi_d^0 = \Xi_d$, for $\ell > 0$ and for any new index $k \in \mathcal{I}_d^\ell \setminus \mathcal{I}_d^{\ell-1}$, we define the knot

$$\xi_{d,k} = \frac{1}{2}(\xi_{d,k-\frac{1}{2^\ell}} + \xi_{d,k+\frac{1}{2^\ell}}),$$

which is well defined because $k - \frac{1}{2^\ell}, k + \frac{1}{2^\ell} \in \mathcal{I}_d^{\ell-1}$. Clearly, $\Xi_d^\ell \subset \Xi_d^{\ell+1}$ for $\ell \geq 0$, and the interval size is $h_{d,\ell} = h_d/2^\ell$. Notice that in this procedure we do not introduce new knots between the repeated knots of the open knot vector.

We also define, for an arbitrary rectangular element in the index domain $\tau = [k_1, k_1 + t_1] \times [k_2, k_2 + t_2]$, with indices $k_d, k_d + t_d \in \mathcal{I}_d^\ell$, the following bisection operators (see [32, Definition 2.5]):

$$\text{bisect}_x(\tau) = \begin{cases} \{[k_1, k_1 + t_1/2] \times [k_2, k_2 + t_2], [k_1 + t_1/2, k_1 + t_1] \times, [k_2, k_2 + t_2]\} & \text{if } \xi_{1,k_1} \neq \xi_{1,k_1+t_1}, \\ \tau & \text{if } \xi_{1,k_1} = \xi_{1,k_1+t_1}, \end{cases}$$

$$\text{bisect}_y(\tau) = \begin{cases} \{[k_1, k_1 + t_1] \times [k_2, k_2 + t_2/2], [k_1, k_1 + t_1] \times, [k_2 + t_2/2, k_2 + t_2]\} & \text{if } \xi_{2,k_2} \neq \xi_{2,k_2+t_2}, \\ \tau & \text{if } \xi_{2,k_2} = \xi_{2,k_2+t_2}. \end{cases}$$

Notice that the bisection operators split the element in two adding a vertical and a horizontal edge, respectively, only when the corresponding length in the parametric domain is greater than zero, that is, when $\xi_{d,k_d+t_d} - \xi_{d,k_d} > 0$.

Starting from the Cartesian grid $\mathcal{T}_0$, we define a T-mesh $\mathcal{T} = \mathcal{T}_N$ by successive applying bisection of elements, in the form

$$\mathcal{T}_{k+1} = \mathcal{T}_k + b_{\tau_k}, \quad \tau_k \in \mathcal{T}_k, \ k = 0, \ldots, N-1, \tag{9}$$

where we use the formal addition (see [32, Definition 2.6] and also [15, Section 3])

$$\mathcal{T}_k + b_{\tau_k} = \mathcal{T}_k \setminus \{\tau_k\} \cup \operatorname{bisect}(\tau_k), \tag{10}$$

and the bisection operator can be either bisect_x or bisect_y. Moreover, we define the finest level Λ as the minimum integer such that the dth coordinate of all vertices in the T-mesh $\mathcal{T}$ belongs to $\mathcal{I}_d^\Lambda$, for $d = 1, 2$.

Remark 4.1 *We notice that a T-mesh defined with this procedure automatically satisfies the first condition in the definition of* admissible mesh *in [6, Definition 7.10], that is, the first $p_d + 1$ lines closer to each boundary are completely contained in the mesh. Instead, the second condition of not having T-junctions in the so-called frame region is not satisfied, because T-junctions may appear on the interface between the frame and the active region. In any case, these T-junctions do not affect the definition of the T-spline functions, and the mesh can still be considered "admissible".*

4.2 Analysis suitable T-splines

To construct the blending functions associated to a T-mesh $\mathcal{T}$, we have to define first the set of *anchors*, that we denote by $\mathcal{A}_{\mathbf{p}}(\mathcal{T})$, and that depends on the degree, see [6, Definition 7.13]. These are either the set of vertices (p_1 and p_2 odd), elements (p_1 and p_2 even), horizontal edges (p_1 even, p_2 odd) or vertical edges (p_1 odd, p_2 even) in the active region, which is the rectangle

$$[\lceil p_1/2 \rceil, m_1 - \lceil p_1/2 \rceil] \times [\lceil p_2/2 \rceil, m_2 - \lceil p_2/2 \rceil],$$

see the examples in Figure 1. We also define the horizontal (resp. vertical) skeleton of the mesh, and denote it by $\operatorname{hSk}(\mathcal{T})$ (resp. $\operatorname{vSk}(\mathcal{T})$), as the union of all horizontal (resp. vertical) edges and vertices. The union of $\operatorname{hSk}(\mathcal{T})$ and $\operatorname{vSk}(\mathcal{T})$ will be called skeleton. Then, for each anchor we construct an ordered horizontal index vector of $p_1 + 2$ indices, tracing a horizontal line from the anchor and collecting the closest $\lfloor (p_1 + 2)/2 \rfloor$ indices leftwards and rightwards where the line intersects the vertical skeleton of the mesh, plus the index of the anchor if the degree is odd, see [6, Definition 7.14] and Figure 1. A vertical index vector of $p_2 + 2$ indices is constructed in an analogous way tracing a vertical line passing through the anchor.

Then, given an anchor $\mathbf{A} \in \mathcal{A}_{\mathbf{p}}(\mathcal{T})$ with horizontal and vertical index vectors

$$hv_{\mathbf{p}}(\mathbf{A}) = \{i_1, \ldots, i_{p_1+2}\} \subset \mathcal{I}_1^\Lambda, \quad vv_{\mathbf{p}}(\mathbf{A}) = \{j_1, \ldots, j_{p_2+2}\} \subset \mathcal{I}_2^\Lambda, \tag{11}$$

we define the local knot vectors

$$\Xi_{\mathbf{A},1,p_1} = \{\xi_{1,i_1}, \ldots, \xi_{1,i_{p_1+2}}\} \subset \Xi_1^\Lambda, \quad \text{and} \quad \Xi_{\mathbf{A},2,p_2} = \{\xi_{2,j_1}, \ldots, \xi_{2,j_{p_2+2}}\} \subset \Xi_2^\Lambda,$$

and from these local knot vectors we define the associated bivariate function

$$B_{\mathbf{A},\mathbf{p}}(\boldsymbol{\zeta}) = B[\Xi_{\mathbf{A},1,p_1}](\zeta_1) B[\Xi_{\mathbf{A},2,p_2}](\zeta_2).$$

We will denote by $S(\mathcal{A}_{\mathbf{p}}(\mathcal{T})) = \operatorname{span}\{B_{\mathbf{A},\mathbf{p}} : \mathbf{A} \in \mathcal{A}_{\mathbf{p}}(\mathcal{T})\}$ the space generated by the T-splines.

A sufficient condition to guarantee linear independence of the T-spline functions is the dual compatibility condition, introduced in [4, 5] and equivalent to the analysis-suitability condition
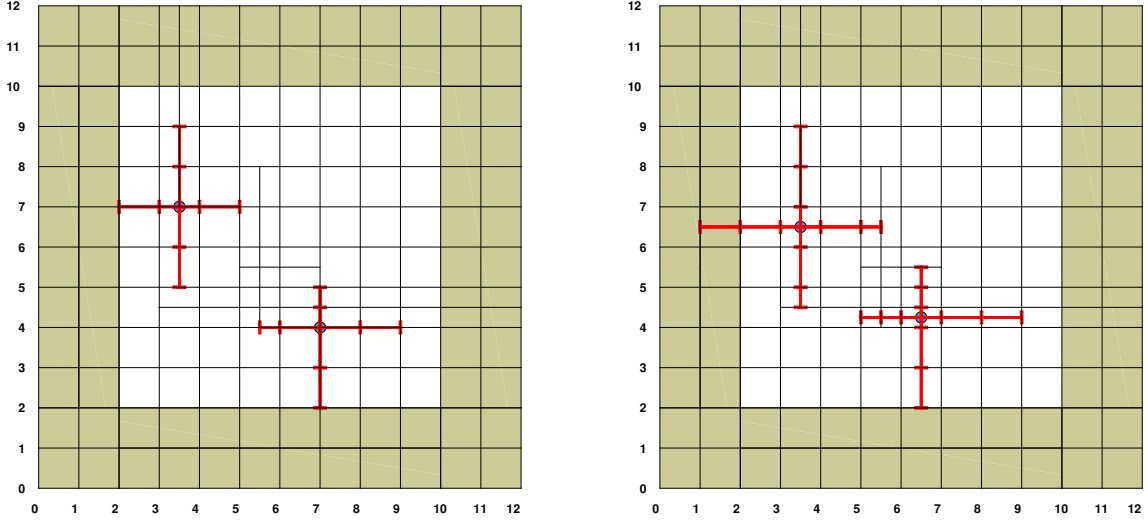
Figure 1: Computation of the index vector for two basis functions, for bicubic (left) and biquartic (right) T-splines

in [30]. The former was generalized to arbitrary dimension in [6]. We say that two local knot vectors *overlap* if both of them can be written as subvectors, with consecutive indices, of the same global knot vector. Then we say that the T-mesh is *dual compatible* if for each pair of anchors $\mathbf{A}', \mathbf{A}'' \in \mathcal{A}_{\mathbf{p}}(\mathcal{T})$, with $\mathbf{A}' \neq \mathbf{A}''$, there exists a direction $d \in \{1, 2\}$ such that the local knot vectors $\Xi_{\mathbf{A}',d,p_d}$ and $\Xi_{\mathbf{A}'',d,p_d}$ are different and overlap. See [6, Section 7.1] for details.

Assuming that the T-mesh is dual compatible, then the functionals

$$\{\lambda_{\mathbf{A},\mathbf{p}}, \mathbf{A} \in \mathcal{A}_{\mathbf{p}}(\mathcal{T})\}, \quad \lambda_{\mathbf{A},\mathbf{p}} := \lambda[\Xi_{\mathbf{A},1,p_1}] \otimes \lambda[\Xi_{\mathbf{A},2,p_2}],$$

form a dual basis for $\{B_{\mathbf{A},\mathbf{p}} : \mathbf{A} \in \mathcal{A}_{\mathbf{p}}(\mathcal{T})\}$ (see [6, Proposition 7.3]). Moreover, we can build the projection operator $\mathbf{\Pi}_{\mathbf{p}}^{\mathcal{T}} \equiv \mathbf{\Pi}_{\mathcal{A}_{\mathbf{p}}(\mathcal{T})} : L^2(\Omega) \to S(\mathcal{A}_{\mathbf{p}}(\mathcal{T}))$ by

$$\mathbf{\Pi}_{\mathbf{p}}^{\mathcal{T}}(f)(\boldsymbol{\zeta}) := \sum_{\mathbf{A} \in \mathcal{A}_{\mathbf{p}}(\mathcal{T})} \lambda_{\mathbf{A},\mathbf{p}}(f) B_{\mathbf{A},\mathbf{p}}(\boldsymbol{\zeta}) \quad \text{for all } f \in L^2(\Omega), \text{ and } \boldsymbol{\zeta} \in \Omega. \tag{12}$$

For the analysis of the projector properties, we make use of the Bézier mesh, that we define as in [6, Section 7.3]. The Bézier mesh is different from the T-mesh, and plays a similar role to the mesh in finite elements. We start recalling that T-junctions are internal vertices of the T-mesh with valence equal to three, that can be grouped in horizontal ($\vdash$, $\dashv$) and vertical ($\top$, $\bot$) T-junctions. For a T-junction of type $\dashv$ with index coordinates $(\bar{\imath}, \bar{\jmath})$, we define the extension as the minimal horizontal line that, passing through the T-junction, intersects $\lfloor p_1/2 \rfloor$ (closed) vertical edges to its left, and $\lceil p_1/2 \rceil$ to its right. The extensions in the other cases are defined in a similar way, using p_2 for vertical T-junctions. Then, we define $\text{ext}_{\mathbf{p}}(\mathcal{T})$ the *extended T-mesh* in the index domain adding to $\mathcal{T}$ all the T-junction extensions. The Bézier mesh $\mathcal{M}^{\mathcal{T}}$ (or simply $\mathcal{M}$) associated to $\mathcal{T}$ is then defined as the collection of *non-empty elements* in the domain Ω of the form

$$Q = (\xi_{1,i_1}, \xi_{1,i_2}) \times (\xi_{2,j_1}, \xi_{2,j_2}) \neq \emptyset, \quad \text{with } (i_1, i_2) \times (j_1, j_2) \in \text{ext}_{\mathbf{p}}(\mathcal{T}).$$

For a Bézier element $Q \in \mathcal{M}^{\mathcal{T}}$, and in general for any subdomain $Q \subset \Omega$, we define the support

extension as the union of the supports of the functions whose support intersects Q, that is

$$\widetilde{Q} := \bigcup_{\mathbf{A} \in \mathcal{A}_Q} \mathrm{supp}(B_{\mathbf{A},\mathbf{p}}), \text{ with } \mathcal{A}_Q = \{\mathbf{A} \in \mathcal{A}_{\mathbf{p}}(\mathcal{T}) : \mathrm{int}(\mathrm{supp}(B_{\mathbf{A},\mathbf{p}})) \cap Q \neq \emptyset\}. \qquad (13)$$

where $\mathrm{int}(C)$ denotes the interior of a set C. Moreover, we define $\bar{Q}$ as the smallest rectangle in Ω containing $\widetilde{Q}$. The following result holds (see [6, Proposition 7.7]):

Proposition 4.1 *Let $\mathcal{T}$ be a dual compatible T-mesh. Then there exists a constant C, depending only on $\mathbf{p}$, such that for any Bézier element $Q \in \mathcal{M}^{\mathcal{T}}$ the projector (12) satisfies*

$$\|\mathbf{\Pi}_{\mathbf{p}}^{\mathcal{T}}(f)\|_{L^2(Q)} \leq C\|f\|_{L^2(\widetilde{Q})}, \text{ for all } f \in L^2(\Omega).$$

Finally, we notice that for each anchor the index vectors (11) define a local Cartesian grid of $(p_1 + 1)(p_2 + 1)$ cells, called *tiled floor* in [4, 5]. Moreover, we also define the *parametric tiled floor*, as the set of non-empty cells

$$[\xi_{1,i_k}, \xi_{1,i_{k+1}}] \times [\xi_{2,j_{k'}}, \xi_{2,j_{k'+1}}] \neq \emptyset, \text{ with } i_k, i_{k+1} \in hv_{\mathbf{p}}(\mathbf{A}), \ j_{k'}, j_{k'+1} \in vv_{\mathbf{p}}(\mathbf{A}).$$

We remark that in general, the cells of the tiled floor do not coincide with the elements of the T-mesh, and the cells of the parametric tiled floor do not coincide with the elements of the Bézier mesh.

4.3 Analysis suitable T-splines by bisection

In order to apply BPX preconditioners to analysis-suitable T-splines, it is necessary to define a suitable refinement procedure that provides a multilevel structure. In this section we adopt the refinement strategy introduced and analysed in [32], and present a new local quasi-uniformity result necessary for the analysis of multilevel preconditioners. The idea in that work is to refine by bisection alternating the refinement direction, and whenever a new edge is added, a recursive algorithm is called to refine the elements in the neighborhood, ensuring that the condition of analysis-suitability is preserved. One of the advantages of this refinement algorithm is that it allows to associate a level (or generation) to each element and function, as required by multilevel methods.

We start setting the *generation* $g(\tau) = 0$ for all the elements of the Cartesian grid $\tau \in \mathcal{T}_0$. Then, the T-mesh $\mathcal{T}$ is defined as in (9)–(10), choosing the bisection

$$\mathrm{bisect}(\tau) = \begin{cases} \mathrm{bisect}_x(\tau) & \text{if } g(\tau) \text{ is even,} \\ \mathrm{bisect}_y(\tau) & \text{if } g(\tau) \text{ is odd,} \end{cases}$$

and setting the generation $g(\tau') = g(\tau) + 1$ for $\tau' \in \mathrm{bisect}(\tau)$ (see [32, Definition 2.6]). Moreover, we say that the bisection b_τ has generation $g(b_\tau) = g(\tau) + 1$. Without loss of generality (see also the proof of Theorem 3.6 in [32]), in the following we will assume that the bisections in (9) are ordered by their generation, that is, if $k > k'$ then $g(b_{\tau_k}) \geq g(b_{\tau_{k'}})$, and the same relation holds for the elements generated by the two bisections. In the following, we will denote by L the finest generation (or level), that is, the generation of the last bisection.

Remark 4.2 *We recall that elements with zero length in one parametric direction are not bisected in that direction, see Section 4.1. However, when applying the bisection operator their generation is increased by one, in such a way that the next time the bisection operator is applied, they will be refined in the other direction.*

To define the generation of the functions, we denote by $\Phi_0 = \{B_{\mathbf{A},\mathbf{p}} : \mathbf{A} \in \mathcal{A}_{\mathbf{p}}(\mathcal{T}_0)\}$ the functions of the tensor product spline space in the coarsest mesh, and then define for $k = 1, \ldots, N$ the collection of T-spline functions newly appeared or modified after the bisection $b_{\tau_{k-1}}$ as

$$\Phi_k := \{B_{\mathbf{A},\mathbf{p}} : \mathbf{A} \in \mathcal{A}_{\mathbf{p}}(\mathcal{T}_k)\} \setminus \{B_{\mathbf{A},\mathbf{p}} : \mathbf{A} \in \mathcal{A}_{\mathbf{p}}(\mathcal{T}_{k-1})\}.$$

Functions in Φ_0 have generation 0, whereas functions in Φ_k have the same generation of the bisection $b_{\tau_{k-1}}$. To alleviate notation, in the following we will denote by ℓ_k the generation (or level) of functions in Φ_k, that is

$$\ell_k := g(b_{\tau_{k-1}}) = g(\tau_{k-1}) + 1, \quad \text{for } k = 0, \ldots, N,$$

with the convention that $g(\tau_{-1}) = -1$. Notice that the subscript k varies from 0 to N, while ℓ_k takes values from 0 to L.

To each Φ_k, we associate a subspace

$$\mathcal{V}_k := \operatorname{span} \Phi_k, \quad 0 \leq k \leq N. \tag{14}$$

We also define the support of functions in $\Phi_k, 1 \leq k \leq N$ and its support extension as

$$\omega_k := \bigcup_{B_{\mathbf{A},\mathbf{p}} \in \Phi_k} \operatorname{supp}(B_{\mathbf{A},\mathbf{p}}), \tag{15}$$

and

$$\widetilde{\omega}_k := \bigcup_{\mathbf{A} \in \mathcal{A}_{\omega_k}} \operatorname{supp}(B_{\mathbf{A},\mathbf{p}}), \text{ with } \mathcal{A}_{\omega_k} := \{\mathbf{A} \in \mathcal{A}_{\mathbf{p}}(\mathcal{T}_k) : \operatorname{int}(\operatorname{supp}(B_{\mathbf{A},\mathbf{p}})) \cap \omega_k \neq \emptyset\}, \tag{16}$$

respectively.

Notice that, since we alternate the directions of refinement, and recalling the notation of Section 4.1, the local knot vectors of a function of generation ℓ are contained in

$$\mathbf{\Xi}^\ell = \{\Xi_1^{\lceil \ell/2 \rceil}, \Xi_2^{\lfloor \ell/2 \rfloor}\}.$$

For convenience, we also introduce the corresponding set of rational indices, $\mathbf{I}^\ell = \{\mathcal{I}_1^{\lceil \ell/2 \rceil}, \mathcal{I}_2^{\lfloor \ell/2 \rfloor}\}$, and the Bézier mesh in the parametric domain $\mathcal{M}_\ell^{\mathcal{B}}$. For each generation ℓ we have that the mesh size is $h_\ell \approx 2^{-\ell/2}$. This important relation between generation and mesh size can be also represented using additional notation as

$$h_\ell \approx \gamma^\ell \quad \text{with } \gamma = 2^{-1/2} \in (0,1).$$

Apart from the generations, that are necessary to provide the multilevel structure, we also need some definitions to adapt the refinement algorithm from [32] to the case of having an open knot vector. Given two points $\mathbf{x}, \mathbf{x}' \in \mathbb{R}^2$ we define the distance between them componentwise as the vector

$$\operatorname{Dist}(\mathbf{x}, \mathbf{x}') = (\operatorname{abs}(x_1 - x_1'), \operatorname{abs}(x_2 - x_2')) \in \mathbb{R}^2.$$

Moreover, let us define, for a point in the index domain $\mathbf{x} = (x_1, x_2) \in [0, m_1] \times [0, m_2]$, its translated version $\widetilde{\mathbf{x}} = (\widetilde{x}_1, \widetilde{x}_2)$ given by

$$\widetilde{x}_d = \begin{cases} p_d & \text{if } x_d < p_d, \\ n_d & \text{if } x_d > n_d, \\ x_d & \text{elsewhere.} \end{cases}$$

Given a bisection T-mesh $\mathcal{T}$ and an element $\tau \in \mathcal{T}$, we denote its middle point as $\mathbf{x}_\tau = (x_{1,\tau}, x_{2,\tau})$. We can define the distance of a point $\mathbf{x}$ to the element τ, and the distance between two elements τ and τ' as

$$\mathrm{Dist}(\mathbf{x}, \tau) := \mathrm{Dist}(\widetilde{\mathbf{x}}, \widetilde{\mathbf{x}}_\tau), \qquad \mathrm{Dist}(\tau, \tau') := \mathrm{Dist}(\widetilde{\mathbf{x}}_\tau, \widetilde{\mathbf{x}}_{\tau'}),$$

respectively. Then, we define the **p**-neighborhood of τ as (see [32, Definition 2.4])

$$\mathcal{G}_\mathbf{p}(\tau) := \{\tau' \in \mathcal{T} : \mathrm{Dist}(\tau, \tau') \leq D_\mathbf{p}(g(\tau))\},$$

where

$$D_\mathbf{p}(\ell) = \begin{cases} 2^{-\ell/2} \left(\lfloor p_1/2 \rfloor + 1/2, \lceil p_2/2 \rceil + 1/2\right) & \text{if } \ell \text{ is even,} \\ 2^{-(\ell+1)/2} \left(\lceil p_1/2 \rceil + 1/2, 2\lfloor p_2/2 \rfloor + 1\right) & \text{if } \ell \text{ is odd.} \end{cases}$$

We also need to define the set (see [32, Corollary 2.15])

$$U_\mathbf{p}(\tau) = \{\mathbf{x} \in [0, m_1] \times [0, m_2] : \mathrm{Dist}(\tau, \mathbf{x}) \leq D_\mathbf{p}(g(\tau))\}.$$

Given a bisection T-mesh $\mathcal{T}$ and an element $\tau \in \mathcal{T}$, we say that the bisection of τ is **p**-admissible or simply admissible, if all $\tau' \in \mathcal{G}_\mathbf{p}(\tau)$ satisfy $g(\tau') \geq g(\tau)$. Moreover, we say that a bisection T-mesh $\mathcal{T}$ is **p**-admissible, if it can be obtained as in (9) with a sequence of admissible bisections. It has been proved in [32, Theorem 3.6] that admissible T-meshes are also analysis suitable, and therefore the dual basis and the projector of the previous section can be built.

Remark 4.3 *The result in [32] does not take into account the repeated knots of the open knot vector. However, the same ideas apply using the definitions above, because the bisection of zero measure elements only adds new lines in the "safe" direction, without causing intersection of T-junction extensions. The use of the translated points in practice forces that a line arriving at a repeated knot, which is on the boundary of the parametric domain, should continue until the boundary of the index domain.*

Besides the analysis suitability condition, we need a local quasi-uniformity result, for which it is necessary to use the following auxiliary lemmas.

Lemma 4.2 *Let $\mathbf{A} \in \mathcal{A}_\mathbf{p}(\mathcal{T})$ be an anchor of a **p**-admissible T-mesh $\mathcal{T}$. Then, any cell in the parametric tiled floor of $\mathbf{A}$ contains at most two Bézier elements of $\mathcal{M}^\mathcal{T}$.*

Proof. Given a cell of the tiled floor, from [5, Lemma 3.2] it does not contain any vertex of $\mathcal{T}$ in its interior, and any line of the extended mesh in its interior belongs to a T-junction extension. Since the mesh is analysis suitable, only vertical or horizontal lines can be found in its interior, but not both. Since a cell in the parametric tiled floor corresponds to a cell in the tiled floor, the result holds because we are refining by bisection alternating the refinement directions. □

Lemma 4.3 *Given a **p**-admissible T-mesh $\mathcal{T}$ and an element $\tau \in \mathcal{T}$, for any $\tau' \in \mathcal{G}_\mathbf{p}(\tau)$ it holds $g(\tau') \geq g(\tau) - 1$.*

Proof. See [32, Lemma 2.14]

Lemma 4.4 *Let $\mathbf{A} \in \mathcal{A}_\mathbf{p}(\mathcal{T})$ be an anchor of a **p**-admissible T-mesh $\mathcal{T}$, associated to a function of generation ℓ. Then the length of the cells of the parametric tiled floor of $\mathbf{A}$ in each parametric direction is equal to*

$$L_1 = \begin{cases} \frac{h_1}{2^{\ell/2}} & \text{if } \ell \text{ is even,} \\ \frac{h_1}{2^{(\ell+1)/2}} & \text{or} \quad \frac{h_1}{2^{(\ell-1)/2}} & \text{if } \ell \text{ is odd,} \end{cases} \qquad L_2 = \begin{cases} \frac{h_2}{2^{\ell/2}} & \text{or} \quad \frac{h_2}{2^{\ell/2-1}} & \text{if } \ell \text{ is even,} \\ \frac{h_2}{2^{(\ell-1)/2}} & \text{if } \ell \text{ is odd.} \end{cases}$$

Proof. The lemma is proved by induction, similarly to [32, Theorem 3.6]. The result clearly holds for the functions in the tensor-product space associated to the T-mesh $\mathcal{T}_0$. Assuming it is true for $\mathcal{T}_k$, we have to prove it for $\mathcal{T}_{k+1} = \mathcal{T}_k + b_{\tau_k}$. Since the bisections can be ordered by their generation, it holds that $\max_{\tau \in \mathcal{T}_k} g(\tau) = g(\tau_k) + 1$. We assume that $g(\tau_k)$ is even, the odd case is proved analogously exchanging the role of the vertical and horizontal directions.

Introducing $\mathcal{T}_\ell^u$ the Cartesian grid obtained after applying all possible bisections of generation ℓ, using the same arguments as in [32, Theorem 3.6], we have the following result about the edges of the T-mesh in the $U_{\mathbf{p}}(\tau_k)$ region

$$\text{hSk}(\mathcal{T}_{k+1}) \cap U_{\mathbf{p}}(\tau_k) = \text{hSk}(\mathcal{T}_{g(\tau_k)}^u) \cap U_{\mathbf{p}}(\tau_k), \tag{17}$$

$$\text{vSk}(\mathcal{T}_{g(\tau_k)}^u) \cap U_{\mathbf{p}}(\tau_k) \subset \text{vSk}(\mathcal{T}_{k+1}) \cap U_{\mathbf{p}}(\tau_k) \subset \text{vSk}(\mathcal{T}_{g(\tau_k)+1}^u) \cap U_{\mathbf{p}}(\tau_k). \tag{18}$$

We have to check that the result is true for the functions introduced or modified by the bisection b_{τ_k}, that is, for functions in Φ_{k+1} of generation $\ell_{k+1} = g(\tau_k) + 1$. Given one of these functions, from the length of the index vectors and (17)–(18) its associated anchor must intersect $U_{\mathbf{p}}(\tau_k)$. Moreover, using [32, Corollary 2.15] this anchor is associated to a geometrical entity (vertex, edge or element) that belongs to an element $\tau' \in \mathcal{G}_{\mathbf{p}}(\tau_k)$. Using first Lemma 4.3 and then the definition of $\mathbf{p}$-admissible T-mesh, for any element $\tau'' \in \mathcal{G}_{\mathbf{p}}(\tau')$ it holds $g(\tau'') \geq g(\tau') - 1 \geq g(\tau_k) - 1$.

Since the horizontal index vector is collected from the vertical lines of elements in $\mathcal{G}_{\mathbf{p}}(\tau')$, in the horizontal direction the intervals of the index vector have lengths at most $2^{-g(\tau_k)/2}$ and $2^{-(g(\tau_k)/2+1)}$, and recalling that $\ell_{k+1} = g(\tau_k) + 1$ is odd, we have the result for the horizontal direction.

For the vertical index vector, following an analogous reasoning we obtain that the intervals in the vertical direction also have lengths $2^{-g(\tau_k)/2}$ and $2^{-(g(\tau_k)/2+1)}$. Moreover, since the anchor of any function in Φ_{k+1} is horizontally aligned with the new edge, using (17) the length of the vertical intervals is always $2^{-g(\tau_k)/2} = 2^{-(\ell_{k+1}-1)/2}$.

Finally, the result is proved passing from the index vectors to the local knot vectors, using the length of the intervals in the knot vectors Ξ_d^ℓ from Section 4.1. $\square$

Corollary 4.5 *In a $\mathbf{p}$-admissible T-mesh, for any basis function $B_{\mathbf{A},\mathbf{p}} \in \Phi_k$, and for any Bézier element $Q \subset \text{supp}(B_{\mathbf{A},\mathbf{p}})$, it holds that $h_Q \approx h_{\ell_k} \approx 2^{-\ell_k/2}$.*

Proposition 4.6 *For a $\mathbf{p}$-admissible T-mesh $\mathcal{T}$, and for any Bézier element $Q \in \mathcal{M}^{\mathcal{T}}$ of the associated Bézier mesh, it holds that $h_Q \approx h_{\widetilde{Q}} \approx h_{\bar{Q}}$.*

Proof. We only need to prove that $h_{\bar{Q}} \lesssim h_{\widetilde{Q}} \lesssim h_Q$, because $Q \subset \widetilde{Q} \subset \bar{Q}$. We start proving $h_{\widetilde{Q}} \lesssim h_Q$. Since the T-mesh is analysis-suitable, in the element Q there are at most $(p_1 + 1)(p_2 + 1)$ basis functions that do not vanish [6, Proposition 7.6], and for each of these functions the element Q is contained in a cell of its parametric tiled floor. Moreover, from Lemma 4.2 this cell contains at most two elements of the Bézier mesh. Finally, each function contains at most $(p_1 + 1)(p_2 + 1)$ cells in its tiled floor, and the result of Lemma 4.4 states that the size of all these cells is comparable. Combining all these results we obtain $h_{\widetilde{Q}} \lesssim h_Q$ with a constant that depends on the degree $\mathbf{p}$.

Let us denote by $h_{1,Q}$ and $h_{2,Q}$ the length of Q and in each parametric direction, and by $h_{1,\widetilde{Q}}$ and $h_{2,\widetilde{Q}}$ the length of $\widetilde{Q}$, given by the difference in the first (second) parametric direction between the rightmost (uppermost) and leftmost (downmost) points in $\widetilde{Q}$. From the previous results and the relative position of the Bézier element inside the tiled floor of each function (see the proof of [6, Proposition 7.6]), we have that

$$(2p_d + 1)h_{d,Q}/2 \leq h_{d,\widetilde{Q}} \leq (2p_d + 1)2h_{d,Q},$$

and since $\bar{Q}$ is the minimum rectangle that contains $\widetilde{Q}$, it also holds that $h_{\bar{Q}} \lesssim h_Q$.

$\square$

Remark 4.4 *For simplicity we have assumed that the internal knots in the knot vectors Ξ_d^ℓ are equally spaced. The results of this section, and in particular Lemma 4.4, can be extended to the case of local quasi-uniform knot vectors under Assumption 3.1.*

Proposition 4.7 *For a $\mathbf{p}$-admissible T-mesh defined as in (9), and for all $u \in L^2(\Omega)$, and $\ell \geq 1$, we have that*

$$\sum_{k:\ell_k=\ell} \|u\|_{\omega_k}^2 \lesssim \|u\|_\Omega^2 \quad and \quad \sum_{k:\ell_k=\ell} \|u\|_{\widetilde{\omega}_k}^2 \lesssim \|u\|_\Omega^2, \tag{19}$$

where ω_k and $\widetilde{\omega}_k$ are as in (15) and (16), respectively.

Proof. The result follows from a careful counting of the number of times a Bézier element Q (or its children, if it is bisected) can appear in the sets ω_k and $\widetilde{\omega}_k$ of the same generation ℓ_k. Studying the worst case scenario, when all the elements in the neighboring of Q are bisected, we see from the graphical explanation in Figure 2 that the element is contained in at most $(2p_1 + 1)(2\lceil p_2/2 \rceil + 1)$ (or $(2p_2 + 1)(2\lceil p_1/2 \rceil + 1)$) sets ω_k.

A similar counting, that can be understood from Figure 3, gives that the element Q is contained in at most $(4p_1+1)(4\lceil p_2/2 \rceil + 2\lfloor p_2/2 \rfloor + 1)$ (or $(4p_2+1)(4\lceil p_1/2 \rceil + 2\lfloor p_1/2 \rfloor + 1)$) sets $\widetilde{\omega}_k$. The result holds with a constant that depends on the degree $\mathbf{p}$.

We remark that in the figures we are mixing Bézier elements and elements in the T-mesh. In this worst case scenario, and staying away from the boundary, there is a one-to-one correspondence between both. $\square$
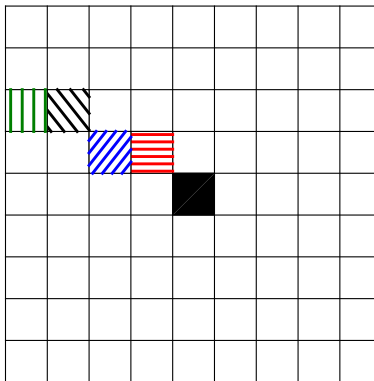

Figure 2: For the chosen element Q (in black), we represent the furthest element τ_k above and to the left such that, when τ_k is bisected, Q is contained in ω_k, for bilinear (red horizontally hatched), biquadratic (blue left diagonally hatched), bicubic (black right diagonally hatched) and biquartic (green vertically hatched).

5   Space decomposition on AS T-meshes

After having introduced all the preliminary results, we are now in a position to prove the main results of the paper, that is, a space decomposition that satisfies **(A1)** and **(A2)**.
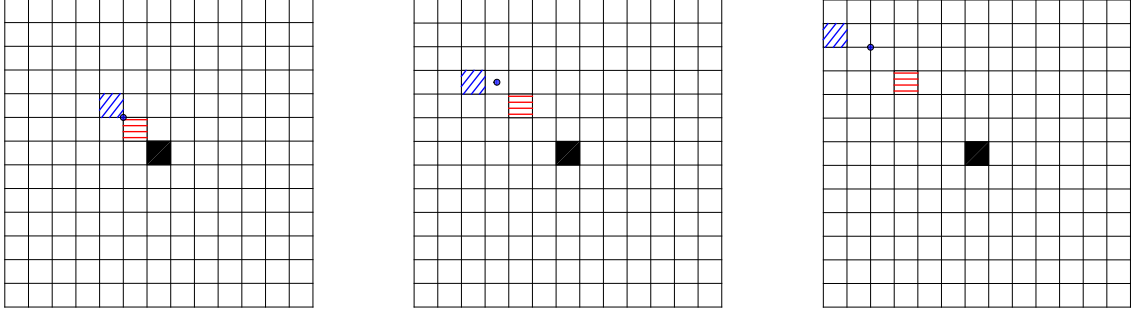
Figure 3: For the chosen element Q (in black), we represent the furthest element Q' (horizontally hatched) such that there is a function that contains both elements in its support, and the furthest element (diagonally hatched) such that its bisection affects a function, anchored at the blue dot, that is in Φ_k and contains Q' in its support. Thus, $Q' \subset \omega_k$ and $Q \subset \widetilde{\omega}_k$. For the bilinear (left), biquadratic (middle) and bicubic (right) cases.

Let $\mathcal{T}$ be a $\mathbf{p}$-admissible T-mesh obtained by successive bisections from the index T-mesh $\mathcal{T}_0$. We give a decomposition of T-splines space $\mathcal{V} := S(\mathcal{A}_{\mathbf{p}}(\mathcal{T}))$ using these successive bisections. By (14), we have the following space decomposition:

$$\mathcal{V} = \sum_{k=0}^{N} \mathcal{V}_k. \tag{20}$$

In each subspace $\mathcal{V}_k$, thanks to Lemma 4.4 and [1], we have the following inverse inequality

$$\|v_k\|_A^2 \lesssim h_{\ell_k}^{-2} \|v_k\|_0^2, \quad \text{for all } v_k \in \mathcal{V}_k, \tag{21}$$

where we recall that h_{ℓ_k} is the mesh size at level ℓ_k, which is the level of functions in Φ_k.

5.1 Stable decomposition

Theorem 5.1 (Space decomposition over AS T-meshes) *For any $v \in \mathcal{V}$, there exist $v_k \in \mathcal{V}_k$, $k = 0, \ldots, N$ such that $v = \sum_{k=0}^{N} v_k$ and*

$$\sum_{k=0}^{N} \|v_k\|_A^2 \lesssim \|v\|_A^2. \tag{22}$$

Proof. First we consider an auxiliary decomposition over uniformly refined spaces of tensor-product B-splines. Let us recall that $\mathcal{T}_\ell^u$ indicates, for $0 \leq \ell \leq L$, the Cartesian mesh obtained after applying all possible bisections of generation ℓ, $S_{\mathbf{p}}(\Xi^\ell)$ is the associated space of tensor-product B-splines of degree $\mathbf{p}$, and $\mathbf{\Pi}_{\mathbf{p},\Xi^\ell} : S_{\mathbf{p}}(\Xi^L) \to S_{\mathbf{p}}(\Xi^\ell)$ is the multivariate quasi-interpolant in (8). We state (without proof) the following well-known stable decomposition for the space $S_{\mathbf{p}}(\Xi^L) = \sum_{\ell=0}^{L} S_{\mathbf{p}}(\Xi^\ell)$ (see [14] for details)

Lemma 5.2 (Stable decomposition for quasi-uniform meshes) *For any $\bar{v} \in S_{\mathbf{p}}(\Xi^L)$, let $\bar{v}_\ell = (\mathbf{\Pi}_{\mathbf{p},\Xi^\ell} - \mathbf{\Pi}_{\mathbf{p},\Xi^{\ell-1}})\bar{v}$ for $\ell = 0, \ldots, L$, setting $\mathbf{\Pi}_{\mathbf{p},\Xi^{-1}} := 0$. Then $\bar{v} = \sum_{\ell=0}^{L} \bar{v}_\ell$ is a stable*

decomposition in the sense that

$$\sum_{\ell=0}^{L} h_\ell^{-2} \|\bar{v}_\ell\|^2 \lesssim |\bar{v}|_1^2. \tag{23}$$

We now give a multilevel decomposition of v using a sequence of projection operators $\mathbf{\Pi}_{\mathbf{p}}^{\mathcal{T}_k}$: $\mathcal{V} \to S(\mathcal{A}_{\mathbf{p}}(\mathcal{T}_k))$, $k = 0, 1, \ldots, N$, which are defined in (12).

First let $v = \sum_{\ell=0}^{L} \bar{v}_\ell$ with $\bar{v}_\ell := (\mathbf{\Pi}_{\mathbf{p}, \mathbf{\Xi}^\ell} - \mathbf{\Pi}_{\mathbf{p}, \mathbf{\Xi}^{\ell-1}})v \in S_{\mathbf{p}}(\mathbf{\Xi}^\ell)$. Then the slicing operator $\mathbf{\Pi}_{\mathbf{p}}^{\mathcal{T}_k} - \mathbf{\Pi}_{\mathbf{p}}^{\mathcal{T}_{k-1}}$ verifies an important property:

$$v_k := (\mathbf{\Pi}_{\mathbf{p}}^{\mathcal{T}_k} - \mathbf{\Pi}_{\mathbf{p}}^{\mathcal{T}_{k-1}})v \ \in \ \mathcal{V}_k \qquad 0 \le k \le N,$$

with the convention that $\mathbf{\Pi}_{\mathbf{p}}^{\mathcal{T}_{-1}} := 0$ and thus $v = \sum_{k=0}^{N} v_k$. If $\ell_k = g(\tau_{k-1}) + 1$ is the generation of the functions in Φ_k, obtained after the bisection of the element τ_{k-1} in (9), then for $l \le \ell_k - 1 = g(\tau_{k-1})$ it holds that $(\mathbf{\Pi}_{\mathbf{p}}^{\mathcal{T}_k} - \mathbf{\Pi}_{\mathbf{p}}^{\mathcal{T}_{k-1}})\bar{v}_l = 0$, which is shown in details in Appendix A.1. Thus for $1 \le k \le N$, we have

$$v_k = (\mathbf{\Pi}_{\mathbf{p}}^{\mathcal{T}_k} - \mathbf{\Pi}_{\mathbf{p}}^{\mathcal{T}_{k-1}}) \sum_{l=\ell_k}^{L} \bar{v}_l.$$

Also, Proposition 4.1 shows that

$$\|v_k\|_{\omega_k}^2 \lesssim \big\| \sum_{l=\ell_k}^{L} \bar{v}_l \big\|_{\widehat{\omega}_k}^2, \qquad 1 \le k \le N.$$

From the definition of the regions ω_k, applying first the inequality above and then inequality (19), we infer that for $\ell \ge 1$

$$\sum_{k:\ell_k=\ell} \|v_k\|^2 = \sum_{k:\ell_k=\ell} \|v_k\|_{\omega_k}^2 \lesssim \sum_{k:\ell_k=\ell} \big\| \sum_{l=\ell_k}^{L} \bar{v}_l \big\|_{\widehat{\omega}_k}^2 \lesssim \big\| \sum_{l=\ell}^{L} \bar{v}_l \big\|_{\Omega}^2 \le \sum_{l=\ell}^{L} \|\bar{v}_l\|_{\Omega}^2.$$

Also we notice that when $\ell = 0$ the space is tensor product, then $v_0 = \bar{v}_0$, and we trivially have

$$\sum_{k:\ell_k=0} \|v_k\|^2 = \|v_0\|_{\Omega}^2 = \|\bar{v}_0\|_{\Omega}^2 \le \sum_{l=0}^{L} \|\bar{v}_l\|_{\Omega}^2.$$

Applying the discrete Hardy inequality [15, Lemma 4.3] with $s = \gamma^2 = 1/2$ to $a_\ell = \|\bar{v}_\ell\|^2$ and $b_\ell = \sum_{k:\ell_k=\ell} \|v_k\|^2$, we obtain

$$\sum_{\ell=0}^{L} h_\ell^{-2} \sum_{k:\ell_k=\ell} \|v_k\|^2 \lesssim \sum_{\ell=0}^{L} h_\ell^{-2} \|\bar{v}_\ell\|^2.$$

Finally, Lemma 5.2 leads to

$$\sum_{k=0}^{N} h_{\ell_k}^{-2} \|v_k\|^2 = \sum_{\ell=0}^{L} h_\ell^{-2} \sum_{k:\ell_k=\ell} \|v_k\|^2 \lesssim \sum_{\ell=0}^{L} h_\ell^{-2} \|\bar{v}_\ell\|^2 \lesssim |v|_1^2.$$

Combining this inequality with (21) gives the desired estimate (22). $\qquad\qquad\square$

5.2 Strengthened Cauchy-Schwarz (SCS) inequality

The proof of the SCS inequality for T-splines relies on the same result for tensor-product B-splines. Although multilevel methods for B-splines are now rather classical, we have not explicitly found the result for tensor-product splines in the literature. For this reason, we start this section proving the SCS inequality in the tensor-product case.

Lemma 5.3 (SCS inequality for B-splines on globally quasi-uniform meshes) *For $u_i \in S_{\mathbf{p}}(\Xi^i)$ and $u_j \in S_{\mathbf{p}}(\Xi^j)$ with $j \geq i$, we have*

$$(u_i, u_j)_A \lesssim \gamma^{(j-i)/2} |u_i|_1 h_j^{-1} \|u_j\|_0,$$

where $\gamma < 1$ is a constant such that $h_i \approx \gamma^i$.

Proof. Recalling that $S_{\mathbf{p}}(\Xi^i) = \mathrm{span}\{B_{\mathbf{i},\mathbf{p}}(\zeta), \ \mathbf{i} \in \mathbf{I}^i\}$ and $S_{\mathbf{p}}(\Xi^j) = \mathrm{span}\{B_{\mathbf{j},\mathbf{p}}(\zeta), \ \mathbf{j} \in \mathbf{I}^j\}$, any $u_j \in S_{\mathbf{p}}(\Xi^j)$ can be written as

$$u_j = \sum_{\mathbf{j} \in \mathbf{I}^j} c_{\mathbf{j},\mathbf{p}} B_{\mathbf{j},\mathbf{p}},$$

which can also be classified as follows: for each Bézier element $Q^i \in \mathcal{M}_i^{\mathcal{B}}$ we define the sets of indices

$$\mathbf{I}_{\mathrm{out}}^j := \{\mathbf{j} \in \mathbf{I}^j : \mathrm{supp}(B_{\mathbf{j},\mathbf{p}}) \cap Q^i = \emptyset\},$$
$$\mathbf{I}_{\mathrm{in}}^j := \{\mathbf{j} \in \mathbf{I}^j : \mathrm{int}(\mathrm{supp}(B_{\mathbf{j},\mathbf{p}})) \subset Q^i\},$$
$$\mathbf{I}_{\mathrm{B}}^j := \{\mathbf{j} \in \mathbf{I}^j : \mathrm{int}(\mathrm{supp}(B_{\mathbf{j},\mathbf{p}})) \cap \partial Q^i \neq \emptyset\},$$

of basis functions with support completely outside of Q^i, completely contained in Q^i, or with just part of it in Q^i, where we recall that the element Q^i is open. Then, we have

$$u_j = u_{\mathrm{out}} + u_{\mathrm{in}} + u_{\mathrm{B}} = \sum_{\mathbf{j} \in \mathbf{I}_{\mathrm{out}}^j} c_{\mathbf{j},\mathbf{p}} B_{\mathbf{j},\mathbf{p}} + \sum_{\mathbf{j} \in \mathbf{I}_{\mathrm{in}}^j} c_{\mathbf{j},\mathbf{p}} B_{\mathbf{j},\mathbf{p}} + \sum_{\mathbf{j} \in \mathbf{I}_{\mathrm{B}}^j} c_{\mathbf{j},\mathbf{p}} B_{\mathbf{j},\mathbf{p}}.$$

Denoting $a_{Q^i}(u,v) := \int_{Q^i} \nabla u \cdot \nabla v \ dx$, we clearly have $a_{Q^i}(u_i, u_{\mathrm{out}}) = 0$, and thus

$$a_{Q^i}(u_i, u_j) = a_{Q^i}(u_i, u_{\mathrm{in}}) + a_{Q^i}(u_i, u_{\mathrm{B}}).$$

Define $\Gamma := \bigcup_{\mathbf{j} \in \mathbf{I}_{\mathrm{B}}^j} \mathrm{supp}(B_{\mathbf{j},\mathbf{p}}) \cap Q^i$, which is the union of smaller elements $Q^j \in \mathcal{M}_j^{\mathcal{B}}$ contained in Q^i and in the support of a function that is not completely contained in Q^i. It is easy to see that $|\Gamma| \approx h_i h_j$, with the implicit constant depending on the degree.

First we estimate the term corresponding to u_{B}. Since $\mathrm{supp}(u_{\mathrm{B}}) \cap Q^i = \Gamma$, we have

$$|a_{Q^i}(u_i, u_{\mathrm{B}})| = |a_{\Gamma}(u_i, u_{\mathrm{B}})| \leq |u_i|_{H^1(\Gamma)} |u_{\mathrm{B}}|_{H^1(\Gamma)}.$$

Using that $\Gamma \subset Q^i$ with $|\Gamma| \approx h_i h_j$, the inverse inequality [11, Lemma 4.5.3], and finally that $h_j \approx \gamma^j$, we obtain

$$
\begin{aligned}
|u_i|_{H^1(\Gamma)} &\leq |\Gamma|^{1/2} |u_i|_{W^{1,\infty}(\Gamma)} \leq |\Gamma|^{1/2} |u_i|_{W^{1,\infty}(Q^i)} \\
&\lesssim |\Gamma|^{1/2} h_i^{-1} |u_i|_{H^1(Q^i)} \lesssim h_j^{1/2} h_i^{1/2} h_i^{-1} |u_i|_{H^1(Q^i)} \\
&\lesssim \gamma^{(j-i)/2} |u_i|_{H^1(Q^i)}.
\end{aligned}
$$

17

The inverse inequality on globally quasi-uniform meshes, followed by [7, Proposition 5.1 and Corollary 5.1] shows that

$$|u_{\mathrm{B}}|_{H^1(\Gamma)} = \sum_{\substack{Q^j \subset \Gamma \\ Q^j \in \mathcal{M}_j^{\mathcal{B}}}} |u_{\mathrm{B}}|_{H^1(Q^j)} \lesssim h_j^{-1} \sum_{\substack{Q^j \subset \Gamma \\ Q^j \in \mathcal{M}_j^{\mathcal{B}}}} \|u_{\mathrm{B}}\|_{L^2(Q^j)} \lesssim h_j^{-1}\|u_{\mathrm{B}}\|_{L^2(\Gamma)} \lesssim h_j^{-1}\|u_j\|_{L^2(Q^i)},$$

where a detailed proof of the last inequality can be found in Appendix A.2. Combining the above two inequalities leads to

$$|a_{Q^i}(u_i, u_{\mathrm{B}})| \lesssim \gamma^{(j-i)/2}|u_i|_{H^1(Q^i)} h_j^{-1}\|u_j\|_{L^2(Q^i)}. \tag{24}$$

Now, for the estimate of the term corresponding to u_{in} we have

$$|a_{Q^i}(u_i, u_{\mathrm{in}})| \leq |(-\Delta u_i, u_{\mathrm{in}})_{L^2(Q^i)}| \leq \|\Delta u_i\|_{L^2(Q^i)}\|u_{\mathrm{in}}\|_{L^2(Q^i)}.$$

It follows from the inverse inequality that

$$\|\Delta u_i\|_{L^2(Q^i)} \lesssim |u_i|_{H^2(Q^i)} \lesssim h_i^{-1}|u_i|_{H^1(Q^i)}.$$

Noting that $\|u_{\mathrm{in}}\|_{L^2(Q^i)} \lesssim \|u_j\|_{L^2(Q^i)}$ that can be shown in a similar way to Appendix A.2, we get

$$\begin{aligned} |a_{Q^i}(u_i, u_{\mathrm{in}})| &\lesssim h_i^{-1}|u_i|_{H^1(Q^i)}\|u_j\|_{L^2(Q^i)} \\ &\lesssim h_j h_i^{-1} h_j^{-1}|u_i|_{H^1(Q^i)}\|u_j\|_{L^2(Q^i)} \\ &\lesssim \gamma^{j-i}|u_i|_{H^1(Q^i)} h_j^{-1}\|u_j\|_{L^2(Q^i)}. \end{aligned} \tag{25}$$

Combining the two estimates (24) and (25), together with $0 < \gamma < 1$, yields

$$|a_{Q^i}(u_i, u_j)| \lesssim \gamma^{(j-i)/2}|u_i|_{H^1(Q^i)} h_j^{-1}\|u_j\|_{L^2(Q^i)}.$$

Summing over Q^i and using the Cauchy inequality, we obtain

$$a(u_i, u_j) \lesssim \gamma^{(j-i)/2}|u_i|_1 h_j^{-1}\|u_j\|_0.$$

which ends the proof. $\qquad\square$

Theorem 5.4 (SCS inequality for AS T-meshes) *For any $u_i, v_i \in \mathcal{V}_i$, $0 \leq i \leq N$, we have*

$$\left|\sum_{i=0}^{N}\sum_{j=i+1}^{N}(u_i, v_j)_A\right| \lesssim \left(\sum_{i=0}^{N}\|u_i\|_A^2\right)^{1/2}\left(\sum_{i=0}^{N}\|v_i\|_A^2\right)^{1/2}.$$

Proof. The proof is similar to the proof of Theorem 4.6 in [15], and is divided into four steps.

1. For a fixed $i \in \{1, 2, \ldots, N\}$, we denote

$$n(i) := \{j > i : \ \omega_j \cap \omega_i \neq \emptyset\} \quad \text{and} \quad w_\ell^i := \sum_{\substack{j \in n(i) \\ j:\ell_j=\ell}} v_j.$$

Observe that $w_\ell^i \in S_{\mathbf{p}}(\mathbf{\Xi}^\ell)$ and $\ell = \ell_j \geq \ell_i$ by the assumption that if $k > k'$, then $\ell_k \geq \ell_{k'}$, while $u_i \in S_{\mathbf{p}}(\mathbf{\Xi}^{\ell_i})$.

For any Bézier element $Q \subset \omega_i$, we apply Lemma 5.3 over Q to u_i and w_ℓ^i to obtain

$$(u_i, w_\ell^i)_{A,Q} \lesssim \gamma^{(\ell-\ell_i)/2} \|u_i\|_{A,Q} \, h_\ell^{-1} \|w_\ell^i\|_{0,Q}.$$

Then

$$
\begin{aligned}
(u_i, w_\ell^i)_{A,\omega_i} = \sum_{Q \subset \omega_i} (u_i, w_\ell^i)_{A,Q} &\lesssim \gamma^{(\ell-\ell_i)/2} \sum_{Q \subset \omega_i} \|u_i\|_{A,Q} \, h_\ell^{-1} \|w_\ell^i\|_{0,Q} \\
&\lesssim \gamma^{(\ell-\ell_i)/2} \|u_i\|_{A,\omega_i} \, h_\ell^{-1} \big(\sum_{Q \subset \omega_i} \|w_\ell^i\|_{0,Q}^2 \big)^{1/2}.
\end{aligned}
$$

Moreover, from the definition of w_ℓ^i

$$\|w_\ell^i\|_{0,Q}^2 \leq \sum_{\substack{j \in n(i) \\ j:\ell_j=\ell}} \|v_j\|_{0,Q}^2 \leq \sum_{j:\ell_j=\ell} \|v_j\|_{0,Q}^2.$$

Thus we obtain

$$(u_i, w_\ell^i)_{A,\omega_i} \lesssim \gamma^{(\ell-\ell_i)/2} \|u_i\|_{A,\omega_i} h_\ell^{-1} \big(\sum_{j:\ell_j=\ell} \|v_j\|_{0,\omega_i}^2 \big)^{1/2}.$$

2. Fix u_i and consider

$$
\begin{aligned}
\big|(u_i, \sum_{j=i+1}^{N} v_j)_A\big| &= \big|(u_i, \sum_{j \in n(i)} v_j)_{A,\omega_i}\big| \\
&= \big|(u_i, \sum_{\ell=\ell_i}^{L} \sum_{\substack{j \in n(i) \\ j:\ell_j=\ell}} v_j)_{A,\omega_i}\big| \leq \sum_{\ell=\ell_i}^{L} \big|(u_i, w_\ell^i)_{A,\omega_i}\big|.
\end{aligned}
$$

Thus we get

$$\big|(u_i, \sum_{j=i+1}^{N} v_j)_A\big| \lesssim \sum_{\ell=\ell_i}^{L} \gamma^{(\ell-\ell_i)/2} \|u_i\|_{A,\omega_i} h_\ell^{-1} \big(\sum_{j:\ell_j=\ell} \|v_j\|_{0,\omega_i}^2 \big)^{1/2}.$$

3. We sum over i with fixed generation $\ell_i = k$:

$$
\begin{aligned}
\sum_{i:\ell_i=k} \big|(u_i, \sum_{j=i+1}^{N} v_j)_A\big| &\lesssim \sum_{i:\ell_i=k} \big(\sum_{\ell=\ell_i}^{L} \gamma^{(\ell-\ell_i)/2} \|u_i\|_{A,\omega_i} h_\ell^{-1} \big(\sum_{j:\ell_j=\ell} \|v_j\|_{0,\omega_i}^2 \big)^{1/2} \big) \\
&\lesssim \sum_{\ell=k}^{L} \gamma^{(\ell-k)/2} \big(\sum_{i:\ell_i=k} \big[\|u_i\|_{A,\omega_i} \big(h_\ell^{-2} \sum_{j:\ell_j=\ell} \|v_j\|_{0,\omega_i}^2 \big)^{1/2} \big] \big) \\
&\lesssim \sum_{\ell=k}^{L} \gamma^{(\ell-k)/2} \big(\sum_{i:\ell_i=k} \|u_i\|_{A,\omega_i}^2 \big)^{1/2} \big(h_\ell^{-2} \sum_{i:\ell_i=k} \sum_{j:\ell_j=\ell} \|v_j\|_{0,\omega_i}^2 \big)^{1/2} \\
&\lesssim \sum_{\ell=k}^{L} \gamma^{(\ell-k)/2} \big(\sum_{i:\ell_i=k} \|u_i\|_{A,\omega_i}^2 \big)^{1/2} \big(h_\ell^{-2} \sum_{j:\ell_j=\ell} \|v_j\|_0^2 \big)^{1/2}.
\end{aligned}
$$

where in the third inequality we used the usual Cauchy-Schwarz inequality and in the last inequality we used Proposition 4.7.

4. Finally we sum over all the generations $0 \le k \le L$ to get

$$\sum_{k=0}^{L}\sum_{i:\ell_i=k}\Big|(u_i,\sum_{j=i+1}^{N}v_j)_A\Big| \lesssim \sum_{k=0}^{L}\Big(\sum_{\ell=k}^{L}\gamma^{(\ell-k)/2}\Big(\sum_{i:\ell_i=k}\|u_i\|_{A,\omega_i}^2\Big)^{1/2}\Big(h_\ell^{-2}\sum_{j:\ell_j=\ell}\|v_j\|_0^2\Big)^{1/2}\Big)$$

$$\lesssim \Big(\sum_{k=0}^{L}\sum_{i:\ell_i=k}\|u_i\|_{A,\omega_i}^2\Big)^{1/2}\Big(\sum_{\ell=0}^{L}h_\ell^{-2}\sum_{j:\ell_j=\ell}\|v_j\|_0^2\Big)^{1/2},$$

where in the last inequality we used the inequality (see [41, Lemma 5])

$$\sum_{i,j=1}^{n}\gamma^{|i-j|}x_iy_j \lesssim \frac{2}{1-\gamma}\Big(\sum_{i=1}^{n}x_i^2\Big)^{1/2}\Big(\sum_{j=1}^{n}y_j^2\Big)^{1/2}, \quad \forall (x_i)_{i=1}^{n},(y_j)_{j=1}^{n}\in\mathbb{R}^n.$$

Since $\sum_{k=0}^{L}\sum_{i:\ell_i=k}=\sum_{i=0}^{N}$, using a scaled Poincaré inequality, namely,

$$h_{\ell_k}^{-2}\|v_k\|_0^2 \lesssim \|v_k\|_A^2, \quad \text{for all } v_k\in\mathcal{V}_k,$$

we have

$$\Big|\sum_{i=0}^{N}\sum_{j=i+1}^{N}(u_i,v_j)_A\Big| \le \sum_{i=0}^{N}\Big|(u_i,\sum_{j=i+1}^{N}v_j)_A\Big| \lesssim \Big(\sum_{i=0}^{N}\|u_i\|_A^2\Big)^{1/2}\Big(\sum_{j=0}^{N}\|v_j\|_A^2\Big)^{1/2}.$$

$\square$

6 BPX preconditioners on locally quasi-uniform AS T-meshes

After the proof of the stable decomposition **(A1)** and the SCS inequality **(A2)**, we can apply the parallel subspace correction method. We introduce two different space decompositions: the first one, that we called *micro decomposition*, is based on the same subspaces in the previous two sections; the second one, that we denote *macro decomposition*, is based on a smaller number of subspaces, that collect all the bisections of the same generation at once.

6.1 Micro decomposition

We apply parallel subspace correction methods to the space decomposition

$$\mathcal{V} = \sum_{k=0}^{N}\mathcal{V}_k, \tag{26}$$

where the subspaces $\mathcal{V}_k$ are defined in (14), and thus obtain BPX preconditioners on locally quasi-uniform AS T-meshes.

Theorem 6.1 *If the preconditioner B of* (3) *is based on the space decomposition* (26) *and the SPD smoothers satisfying* (4)*, then we have*

$$\kappa(BA) \lesssim 1.$$

Proof. It follows immediately from Theorems 5.1, 5.4 and 2.1. $\square$

Remark 6.1 *We observe that we can use standard smoothers such as Jacobi and symmetric Gauss-Seidel iterations satisfying (4). Recently, Hofreither et al. in [24] proposed a new smoother based on the mass matrix and a boundary correction, and showed that on a uniform mesh, the multigrid with the new smoother has the robust convergence independent of both the mesh size and the spline degree. The extension of this smoother to T-splines is one of our future research topics. We notice however that this would eliminate the dependency on the degree for K_3 and K_4 in (5), but not for K_1 and K_2.*

6.2 Macro decomposition

As an alternative to the previous decomposition, we introduce a *macro* space decomposition where each level contains all the elements of the same corresponding generation. In order to define the macro space decomposition, to each generation ℓ we associate a subspace $\mathcal{W}_\ell$ that contains the functions added or modified after inserting all the lines of generation ℓ. For instance, in the T-meshes of Figure 4, $\mathcal{W}_0$ would be the tensor-product space in the *black* mesh, and the subspaces $\mathcal{W}_1$, $\mathcal{W}_2$ and $\mathcal{W}_3$ would consist of the T-splines added or modified after the bisection sequence for adding all the *red* vertical edges, all the *blue* horizontal edges, and all the *pink* vertical edges, respectively.

To be more precise, starting from the Cartesian mesh $\mathcal{T}_0$, we define for $1 \leq \ell \leq L$ the T-mesh

$$\overline{\mathcal{T}}_\ell := \mathcal{T}_{k(\ell)}, \qquad \text{with} \quad k(\ell) := \max\{k : \ell_k = \ell \text{ with } \ell_k := g(b_{\tau_{k-1}})\},$$

which is the finest T-mesh of generation ℓ. Similarly to the sets Φ_k in Section 4.3, we can now define the sets

$$\overline{\Phi}_\ell := \{B_{\mathbf{A},\mathbf{p}} : \mathbf{A} \in \mathcal{A}_\mathbf{p}(\overline{\mathcal{T}}_\ell)\} \backslash \{B_{\mathbf{A},\mathbf{p}} : \mathbf{A} \in \mathcal{A}_\mathbf{p}(\overline{\mathcal{T}}_{\ell-1})\},$$

and the subspace

$$\mathcal{W}_\ell := \text{span } \overline{\Phi}_\ell,$$

noting that this subspace contains all the subspaces of the micro decomposition of the corresponding generation, in fact, $\mathcal{W}_\ell = \sum_{k:\ell_k=\ell} \mathcal{V}_k$.

Defining those $\mathcal{W}_\ell$ gives the decomposition

$$\mathcal{V} = \sum_{\ell=0}^{L} \mathcal{W}_\ell. \tag{27}$$

We can use the general framework presented in Sections 4-5 to obtain the uniformly bounded condition number of the BPX preconditioner on the macro space decomposition (27).

Remark 6.2 *It is worth to mention that since our macro structure is similar to the locally refined grids proposed in [9, 10, 40], BPX optimality on the space decomposition (27) can also be obtained in an analogous way to the proofs in those references.*

6.3 Application to IGA

All the theoretical results presented in this paper are proved in the unit domain $\Omega = (0,1)^2$. The results can be easily extended to the IGA setting, where the physical domain Ω is defined as the image of the unit parametric domain through a parametrization $\mathbf{F}$, that is, $\Omega = \mathbf{F}((0,1)^2)$. The parametrization $\mathbf{F}$ can be defined as a T-spline on a coarse mesh, and both $\mathbf{F}$ and its inverse should be regular, see [14] for details.

7 Numerical results

We have performed some numerical tests to support our theoretical results with numerical evidence. We solve the model problem (1) with a suitable f that makes it necessary to refine towards a corner, noticing however that the condition number does not depend on f. Since we lack a true implementation of T-splines, we have run the tests using the Octave/Matlab software GeoPDEs [18, 37] for some particular T-meshes, defining a tensor-product space for each level, and then collecting the active functions of different levels. Our implementation is clearly unefficient for T-splines, hence we do not present computational times.

7.1 Macro tests

In the first two tests we follow the *macro* space decomposition in Section 6.2, that is, the subspace $\mathcal{W}_k$ contains the functions that have been added or modified after inserting all the lines of generation k.

7.1.1 Square domain

In the first test the domain is the unit square $\Omega_0 = (0,1)^2$, which is refined near the origin with the following procedure: the level zero mesh is a Cartesian grid, and then for each level we refine, in the T-mesh, the maximal square subregion such that the T-mesh remains **p**-admissible in the sense of [32]. The number of elements of the initial Cartesian grid has been chosen to obtain a similar number of degrees of freedom for each degree. In particular, it is equal to 7^2, 8^2 and 10^2 for biquadratic, bicubic and biquartic splines, respectively. We show in Figure 4 the refined meshes for the biquadratic and the bicubic case, after all the bisections of the fourth generation.

For the computations with the BPX preconditioner, the inclusion operator I_k can be computed through knot insertion, while the restriction operator is simply its transpose. We have compared the results with two different smoothers R_k: Jacobi and symmetric Gauss-Seidel, with one single iteration each. The condition number of the preconditioned system is estimated computing the minimum and maximum eigenvalues with Lanczos' method. The stopping criterion is set to an initial tolerance of 10^{-6} for coarse meshes. Table 1 summarizes the obtained results, where the number of degrees of freedom corresponds to the matrix size, that is, after applying Dirichlet boundary conditions.

As predicted by the theory, the numerical results show that the condition number remains bounded by a constant during h-refinement. As already observed in [14], the constant deteriorates with the degree p, and as explained in [24] (see also [20]) this is due to the bad behavior of Jacobi and symmetric Gauss-Seidel smoothers with splines. The smoother recently proposed in [24] can be probably adapted to AS T-splines by bisection, but it is beyond the scope of this paper. We also remark that, although the condition number is lower using symmetric Gauss-Seidel as a smoother, the iteration cost in our implementation is higher, thus in our tests the Jacobi smoother performs better than the Gauss-Seidel one.

7.1.2 Curved L-shaped domain

As a second test we have considered the curved L-shaped domain in Figure 5. The domain is defined with three patches, each one the image of the unit square through a different parametrization $\mathbf{F}$, in such a way that the reentrant corner is always the image of the origin. We have constructed, in the parametric domain, the same meshes as in the previous test, which are then mapped to the physical
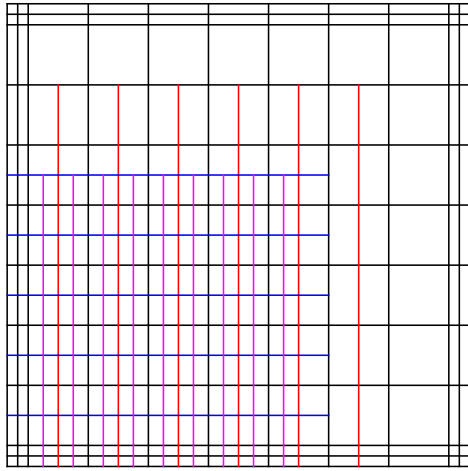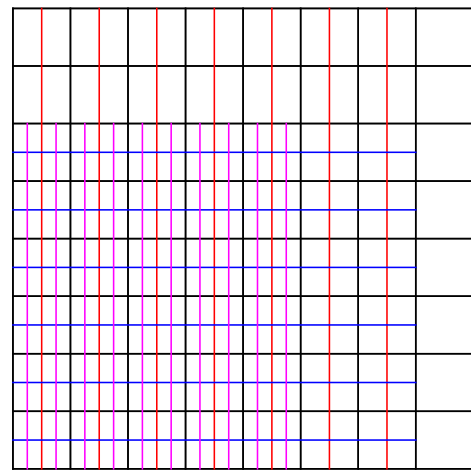
(a) T-mesh, $p = 2$
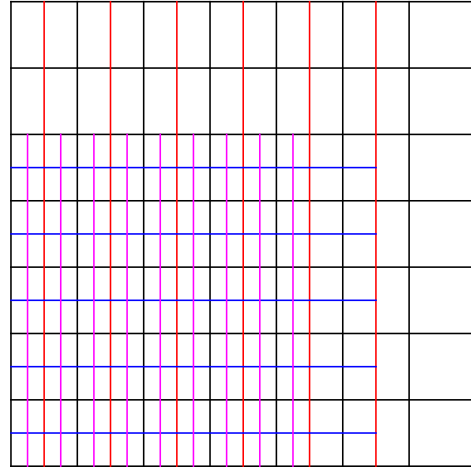
(b) Bézier mesh, $p = 2$
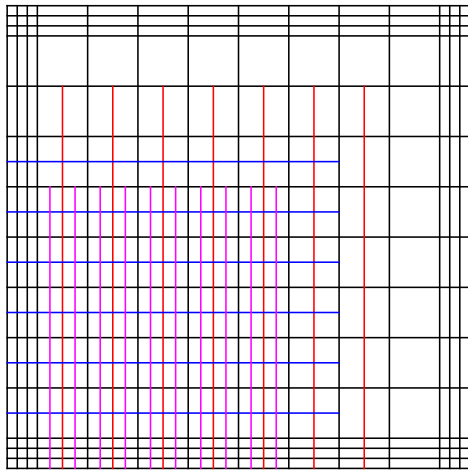
(c) T-mesh, $p = 3$

(d) Bézier mesh, $p = 3$

Figure 4: The fourth generation T-meshes in the first numerical test, and the corresponding Bézier meshes, for $p = 2$ and $p = 3$. For interpretation of the references to color in this figure legend, the reader is referred to the web version of this article

23

	Biquadratic				Bicubic				Biquartic			
Levels	Dofs	N.P.	Jac.	GS	Dofs	N.P.	Jac.	GS	Dofs	N.P.	Jac.	GS
2	85	14.8	8.0	2.7	137	48.3	33.8	6.6	234	373.9	167.7	23.9
3	135	23.7	10.6	3.5	215	33.6	56.7	7.6	339	272.1	294.5	35.4
4	216	46.5	14.7	5.3	325	64.6	74.2	13.2	495	373.1	393.7	46.5
5	344	74.2	16.7	6.0	496	75.2	88.4	12.9	705	299.6	494.7	58.8
6	569	139.3	20.6	7.5	768	181.0	103.6	19.7	1047	378.4	572.2	67.0
7	961	234.5	20.4	7.6	1233	217.6	109.6	20.4	1575	313.8	642.8	82.6
8	1690	447.7	23.2	8.7	2045	540.6	123.6	24.9	2505	737.3	694.3	86.0
9	3042	798.9	22.1	8.5	3530	686.1	124.3	24.8	4101	918.9	743.1	103.6
10	5643	1560.9	24.6	9.4	6286	1785.7	133.2	27.9	7071	2286.9	770.1	108.7
11	10643	2907.2	23.1	9.1	11539	2371.1	133.9	27.4	12531	3030.4	805.1	118.1
12	20444	5770.1	25.5	9.8	21639	6382.3	140.8	29.9	23037	7868.2	816.5	121.1
13	39652	11040.6	24.0	9.4	41340	8729.9	140.4	29.4	43137	10855.7	843.2	127.1
14	77677	22109.3	26.2	9.9	79952	23983.8	145.9	31.2	82539	28931.9	846.6	128.1
15	152949	42979.9	24.6	9.6	156197	33390.6	145.0	30.6	159567	40886.2	867.2	132.7

Table 1: Condition numbers for the square domain. N.P: no preconditioner. Jac: Jacobi smoother. GS: Gauss-Seidel smoother

domain through $\mathbf{F}$. The relative orientation of the three patches guarantees that the meshes match on the interfaces, and basis functions on the interfaces are glued together with C^0 continuity.

We have run the same kind of tests as before, the results are summarized in Table 2. The numerical results show that the presence of the parametrization does not greatly affect the condition number, as long as the parametrization remains regular. These results are in agreement with those in [14] for tensor-product B-splines.

7.2 Comparison with other variants

7.2.1 Micro test

Our implementation is not general enough to test the preconditioner using the *micro* technique, that is, defining the decomposition spaces $\mathcal{V}_k$ as in (14). However, in order to better understand how it could work we have tried a modified version of the method: instead of adding all the bisections of the same generation at the same time, as in the *macro* technique, we group aligned bisection edges of the same generation into one single level. For instance, in the example of Figure 4(c) for the bicubic case, and recalling that we start from generation zero, the first, second and third generations contain seven, six and ten new levels, respectively.

The tests have been run only for the bicubic case. In Table 3 we show the condition numbers of the system obtained after all the lines of the same generation have been obtained, that can be compared with the ones obtained with the macro technique in Table 1. Although the condition number remains bounded, as predicted by the theory, the results show a loss of efficiency of the preconditioner. This is probably due to the smaller number of degrees of freedom that are added at each level in the micro decomposition with respect to the macro one.

7.2.2 An alternative refinement

In all the previous tests the refinement is performed as in [32] to obtain **p**-admissible meshes, that is, the elements are refined alternatively in the vertical and the horizontal direction, depending on

Levels	Biquadratic				Bicubic				Biquartic			
	Dofs	N.P.	Jac.	GS	Dofs	N.P.	Jac.	GS	Dofs	N.P.	Jac.	GS
2	275	60.7	10.2	2.8	436	122.6	47.1	6.7	735	1060.8	233.4	23.9
3	430	80.0	16.2	4.0	676	147.9	82.0	9.9	1057	744.6	394.5	36.5
4	682	202.4	22.6	5.6	1016	368.5	113.8	13.4	1537	1048.1	581.4	48.9
5	1074	270.5	27.5	6.6	1538	478.7	145.9	16.7	2177	870.5	756.6	61.6
6	1764	654.7	32.8	8.0	2370	1117.5	172.9	20.1	3221	1963.0	910.3	74.5
7	2954	914.5	36.3	8.5	3780	1509.3	198.4	22.7	4821	2506.6	1047.1	86.0
8	5168	2203.6	41.1	9.6	6244	3510.3	220.3	25.6	7641	5633.6	1168.9	97.9
9	9250	3238.5	43.6	9.7	10726	5013.1	240.2	27.4	12457	7710.7	1276.9	106.5
10	17104	7864.6	47.8	10.6	19046	11862.7	258.5	29.4	21421	17773.4	1375.3	116.2
11	32154	12027.0	49.8	10.5	34856	17793.4	275.0	30.4	37853	25944.3	1461.5	122.0
12	61656	29424.9	53.5	11.3	65256	42832.1	290.1	31.9	69473	61381.7	1541.2	129.2
13	119378	46178.5	54.9	11.1	124458	66460.2	303.5	32.4	129873	93799.5	1610.5	132.5

Table 2: Condition numbers for the curved L-shaped domain. N.P: no preconditioner. Jac: Jacobi smoother. GS: Gauss-Seidel smoother

Levels	Dofs	N.P.	Jac	GS
8 (2)	137	48.3	57.8	13.2
14 (3)	215	33.6	112.6	23.7
24 (4)	325	64.6	145.9	31.1
33 (5)	496	75.2	182.5	42.9
49 (6)	768	181.0	198.5	45.9
64 (7)	1233	217.6	220.6	56.2
92 (8)	2045	540.6	232.6	56.6
119 (9)	3530	686.1	247.2	67.1
171 (10)	6286	1785.7	252.2	63.5
222 (11)	11539	2371.1	260.7	72.2
322 (12)	21639	6382.3	264.1	66.3
421 (13)	41340	8729.9	270.4	74.2
617 (14)	79952	23983.8	272.1	67.8

Table 3: Condition number obtained with the *micro* technique, after adding all the lines of the same generation (between parentheses)
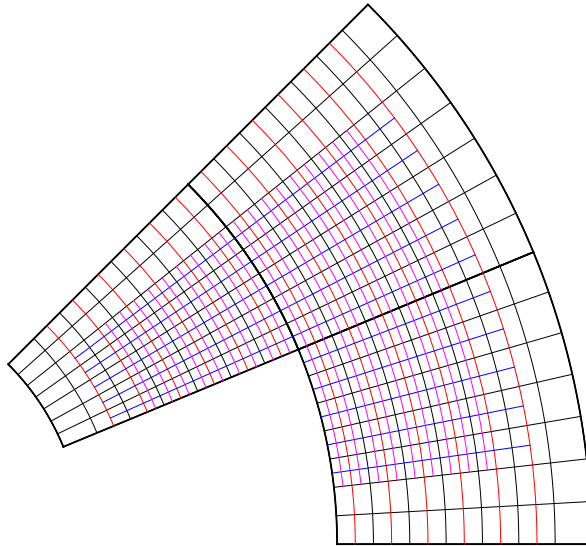
Figure 5: Bézier mesh of the curved L-shaped domain with four levels, biquadratic case. For interpretation of the references to color in this figure legend, the reader is referred to the web version of this article

their generation. For this new test we have tried a different kind of refinement that, preserving the multilevel structure and the analysis-suitability, provides more regular elements. Starting from a Cartesian grid, the elements of the T-mesh in a square subregion next to the corner are split in four, bisecting them vertically and horizontally simultaneously. Then, some other elements have to be bisected, either horizontally or vertically, to maintain the analysis-suitability property. To simplify the computations, in this second step we refine together a set of aligned elements, although this is not really necessary to maintain the analysis-suitable property. All the functions added or modified during the refinement of the square region are considered to have the same generation, independently of whether the refinement is horizontal, vertical or both. A detail of the meshes obtained after three refinement steps, for the biquadratic case, is shown in Figure 6. Lines added at the same step are drawn with the same color.

For the numerical tests we use the *macro* technique as in Section 7.1, that is, the space $\mathcal{W}_k$ is defined after adding all the lines of the same generation. In Table 4 we show the results obtained applying the BPX preconditioner with this kind of refinement. The results show a better behavior of the BPX preconditioner compared to the meshes in Section 7.1, and in fact the numbers are very similar to the ones obtained for tensor-product B-splines in [14]. Indeed, this seems a good motivation to look for alternative refinement techniques for T-splines, that are less restrictive than the one in [32]. This may be possible after the definition of truncated T-splines [39], for which has been proved linear independence with a less restrictive condition than the one of analysis-suitable T-splines.
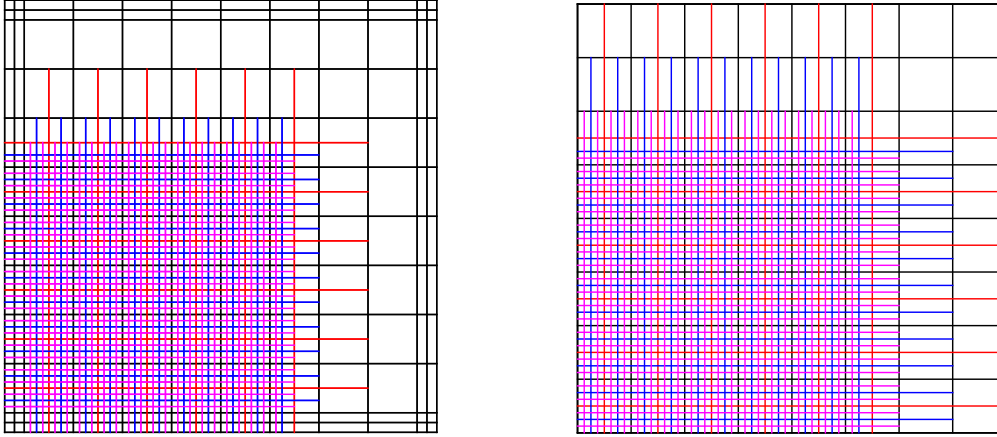
Acknowledgments

Figure 6: The alternative refinement for the biquadratic case: T-mesh (left) and corresponding Bézier mesh (right). For interpretation of the references to color in this figure legend, the reader is referred to the web version of this article

Levels	Biquadratic				Bicubic				Biquartic			
	Dofs	N.P.	Jac.	GS	Dofs	N.P.	Jac.	GS	Dofs	N.P.	Jac.	GS
2	184	23.4	6.4	2.4	213	33.5	30.0	5.9	244	243.3	134.6	19.8
3	569	103.5	10.2	3.6	620	126.6	48.8	9.0	673	390.8	285.8	34.8
4	1934	402.8	11.3	4.4	2027	608.9	60.5	12.0	2122	853.1	368.3	47.0
5	7059	1530.0	12.0	4.9	7234	2542.9	65.2	14.0	7411	4318.7	409.0	57.2
6	26904	5999.2	12.3	5.0	27241	10270.6	67.3	15.0	27580	18742.2	423.4	63.5
7	104989	23738.0	12.5	5.1	105648	41233.4	68.9	15.6	106309	77464.3	427.3	67.0

Table 4: Condition numbers with the alternative refinement. N.P: no preconditioner. Jac: Jacobi smoother. GS: Gauss-Seidel smoother

A Mathematical proofs of auxiliary results

A.1 Difference of T-spline projectors applied to coarse B-splines

The first auxiliary result was used in the proof of Theorem 5.1. Letting $\bar{v}_\ell := (\mathbf{\Pi}_{\mathbf{p},\mathbf{\Xi}^\ell} - \mathbf{\Pi}_{\mathbf{p},\mathbf{\Xi}^{\ell-1}})v \in S_{\mathbf{p}}(\mathbf{\Xi}^\ell)$, $0 \leq \ell \leq L$, we need to prove that for $l \leq \ell_k - 1$

$$(\mathbf{\Pi}_{\mathbf{p}}^{\mathcal{T}_k} - \mathbf{\Pi}_{\mathbf{p}}^{\mathcal{T}_{k-1}})\bar{v}_l = 0,$$

which is a consequence of the following lemma.

Lemma A.1 *Let* $\mathcal{T}_k = \mathcal{T}_{k-1} + b_{\tau_{k-1}}$ *be a* **p**-*admissible T-mesh generated by bisection of* τ_{k-1}, *and let* $\ell_k = g(\tau_{k-1}) + 1$. *Then it holds that*

$$(\mathbf{\Pi}_{\mathbf{p}}^{\mathcal{T}_k} - \mathbf{\Pi}_{\mathbf{p}}^{\mathcal{T}_{k-1}})v = 0$$

for any function $v \in S_{\mathbf{p}}(\mathbf{\Xi}^{\ell})$, *with* $\ell < \ell_k$.

Proof. Since $S_{\mathbf{p}}(\mathbf{\Xi}^i) \subset S_{\mathbf{p}}(\mathbf{\Xi}^j)$ for $i \leq j$, we only need to prove the result for a function $v \in S_{\mathbf{p}}(\mathbf{\Xi}^{\ell_k - 1})$. Let us first define, similarly to Φ_k, the set

$$\Psi_{k-1} := \{B_{\mathbf{A},\mathbf{p}} : \mathbf{A} \in \mathcal{A}_{\mathbf{p}}(\mathcal{T}_{k-1})\} \setminus \{B_{\mathbf{A},\mathbf{p}} : \mathbf{A} \in \mathcal{A}_{\mathbf{p}}(\mathcal{T}_k)\},$$

which is the collection of functions removed after the bisection $b_{\tau_{k-1}}$. Since the bisection only affects basis functions in Ψ_{k-1} (removed) and Φ_k (added), from the definition of the dual functionals it is clear that

$$(\mathbf{\Pi}_{\mathbf{p}}^{\mathcal{T}_k} - \mathbf{\Pi}_{\mathbf{p}}^{\mathcal{T}_{k-1}})v = \sum_{\mathbf{A}:B_{\mathbf{A},\mathbf{p}} \in \Phi_k} (\lambda_{\mathbf{A},\mathbf{p}}v)B_{\mathbf{A},\mathbf{p}} - \sum_{\mathbf{A}:B_{\mathbf{A},\mathbf{p}} \in \Psi_{k-1}} (\lambda_{\mathbf{A},\mathbf{p}}v)B_{\mathbf{A},\mathbf{p}}.$$

From the nestedness of the T-spline spaces $S(\mathcal{A}_{\mathbf{p}}(\mathcal{T}_{k-1})) \subset S(\mathcal{A}_{\mathbf{p}}(\mathcal{T}_k))$ (see [32, Corollary 5.8]), it holds that $\operatorname{span}(\Psi_{k-1}) \subset \operatorname{span}(\Phi_k)$, and by the local linear independence of analysis-suitable T-splines, we have

$$\bigcup_{B_{\mathbf{A},\mathbf{p}} \in \Psi_{k-1}} \operatorname{supp}(B_{\mathbf{A},\mathbf{p}}) \subset \bigcup_{B_{\mathbf{A},\mathbf{p}} \in \Phi_k} \operatorname{supp}(B_{\mathbf{A},\mathbf{p}}) = \omega_k.$$

Moreover, from Lemma 4.4, and in particular from (17)-(18), we know that functions in Φ_k see all the lines of the uniform Cartesian mesh $\mathcal{T}_{\ell_k-1}^u$ in the vicinity of τ_{k-1}, and using the previous property for the supports, we know that the same is true for functions in Ψ_{k-1}.

Let us define, starting from the uniform Cartesian mesh $\mathcal{T}_0' = \mathcal{T}_{\ell_k-1}^u$ the auxiliary family of **p**-admissible T-meshes

$$\mathcal{T}_{j+1}' = \mathcal{T}_j' + b_{\tau_{j+k_0}}, \quad j = 0, \ldots, k - k_0 - 1,$$

where k_0 is the minimum integer such that $g(\tau_{k_0}) = g(\tau_{k-1})$ in the construction (9) of the T-mesh $\mathcal{T}_{k+1}$. In other words, starting from the Cartesian grid of level $\ell_k - 1$, we perform the bisections of the same generation until we reach $b_{\tau_{k-1}}$. From what we have just seen, it is clear that $\Phi_{k-k_0}' = \Phi_k$ and $\Psi_{k-k_0-1}' = \Psi_{k-1}$, and by the nestedness of **p**-admissible T-splines it holds $S_{\mathbf{p}}(\mathbf{\Xi}^{\ell_k-1}) = S(\mathcal{A}_{\mathbf{p}}(\mathcal{T}_0')) \subset S(\mathcal{A}_{\mathbf{p}}(\mathcal{T}_j'))$ for any $j = 0, \ldots, k - k_0$. Thus we have, for $v \in S_{\mathbf{p}}(\mathbf{\Xi}^{\ell_k-1})$

$$0 = \left(\mathbf{\Pi}_{\mathbf{p}}^{\mathcal{T}_{k-k_0}'} - \mathbf{\Pi}_{\mathbf{p}}^{\mathcal{T}_{k-k_0-1}'}\right)v = \sum_{\mathbf{A}:B_{\mathbf{A},\mathbf{p}} \in \Phi_{k-k_0}'} (\lambda_{\mathbf{A},\mathbf{p}}v)B_{\mathbf{A},\mathbf{p}} - \sum_{\mathbf{A}:B_{\mathbf{A},\mathbf{p}} \in \Psi_{k-k_0-1}'} (\lambda_{\mathbf{A},\mathbf{p}}v)B_{\mathbf{A},\mathbf{p}},$$

which ends the proof. $\qquad\square$

A.2 Appropriate discrete norms

The second auxiliary result, that we present in this subsection, is $\|u_{\mathrm{B}}\|_{L^2(\Gamma)} \lesssim \|u_j\|_{L^2(Q^i)}$ in the proof of Lemma 5.3.

Let $Q^i \in \mathcal{M}_i^{\mathcal{B}}$ be a Bézier element of the Cartesian grid of generation i. For $j \geq i$ we define the set of indices

$$\mathbf{I}^j(Q^i) := \{\mathbf{j} \in \mathbf{I}^j : \operatorname{supp}(B_{\mathbf{j},\mathbf{p}}) \cap Q^i \neq \emptyset\},$$

which is also the union of indices $\mathbf{I}^j_{\text{in}}$ and $\mathbf{I}^j_{\text{B}}$ defined as in the proof of Lemma 5.3, namely, $\mathbf{I}^j(Q^i) = \mathbf{I}^j_{\text{in}} \cup \mathbf{I}^j_{\text{B}}$. By local linear independence of B-splines, a function $z \in S_{\mathbf{p}}(\boldsymbol{\Xi}^j)$ restricted to Q^i can be written as

$$z|_{Q^i} = \sum_{\mathbf{j} \in \mathbf{I}^j(Q^i)} c_{\mathbf{j}} B_{\mathbf{j},\mathbf{p}}.$$

Let also $Q^j \in \mathcal{M}^{\mathcal{B}}_j$ such that $Q^j \subset Q^i$, and define $\mathbf{I}^j(Q^j) := \{\mathbf{j} \in \mathbf{I}^j : Q^j \subset \text{supp}(B_{\mathbf{j},\mathbf{p}})\}$. Obviously, $\mathbf{I}^j(Q^j) \subset \mathbf{I}^j(Q^i)$. We define a local discrete norm $|\cdot|_{Q^j}$ as follows: for any $z \in S_{\mathbf{p}}(\boldsymbol{\Xi}^j)|_{Q^i}$,

$$|z|^2_{Q^j} := \left(\max_{\mathbf{j} \in \mathbf{I}^j(Q^j)} |c_{\mathbf{j}}|^2 \right) h_j^2,$$

and also define the global discrete norm $|\cdot|_{Q^i}$ on Q^i as follows: for any $z \in S_{\mathbf{p}}(\boldsymbol{\Xi}^j)|_{Q^i}$,

$$|z|^2_{Q^i} := \sum_{\mathbf{j} \in \mathbf{I}^j(Q^i)} |c_{\mathbf{j}}|^2 h_j^2.$$

Proposition A.1 *Let $Q^i \in \mathcal{M}^{\mathcal{B}}_i$ and let, for $j \geq i$, $Q^j \in \mathcal{M}^{\mathcal{B}}_j$ such that $Q^j \subset Q^i$. Then for any $z \in S_{\mathbf{p}}(\boldsymbol{\Xi}^j)|_{Q^i}$ it holds*

$$\|z\|^2_{L^2(Q^j)} \approx |z|^2_{Q^j},$$

and

$$\|z\|^2_{L^2(Q^i)} \approx |z|^2_{Q^i}.$$

Proof. The proof can be found in [7, Proposition 5.1 and Corollary 5.1]. $\qquad\square$

By Proposition A.1, it is clear that

$$\|u_{\text{B}}\|_{L^2(\Gamma)} \lesssim \|u_j\|_{L^2(Q^i)}.$$

References

[1] Y. BAZILEVS, L. BEIRÃO DA VEIGA, J. A. COTTRELL, T. J. R. HUGHES, AND G. SANGALLI, *Isogeometric analysis: approximation, stability and error estimates for h-refined meshes*, Math. Models Methods Appl. Sci., 16 (2006), pp. 1031–1090.

[2] Y. BAZILEVS, V. CALO, J. A. COTTRELL, J. A. EVANS, T. J. R. HUGHES, S. LIPTON, M. SCOTT, AND T. SEDERBERG, *Isogeometric analysis using T-splines*, Comput. Methods Appl. Mech. Engrg., 199 (2010), pp. 229 – 263.

[3] L. BEIRÃO DA VEIGA, L. F. PAVARINO, S. SCACCHI, O. B. WIDLUND, AND S. ZAMPINI, *Isogeometric BDDC preconditioners with deluxe scaling*, SIAM J. Sci. Comput., 36 (2014), pp. A1118–A1139.

[4] L. BEIRÃO DA VEIGA, A. BUFFA, D. CHO, AND G. SANGALLI, *Analysis-Suitable T-splines are Dual-Compatible*, Comput. Methods Appl. Mech. Engrg., 249–252 (2012), pp. 42 – 51.

[5] L. BEIRÃO DA VEIGA, A. BUFFA, G. SANGALLI, AND R. VÁZQUEZ, *Analysis-suitable T-splines of arbitrary degree: Definition, linear independence and approximation properties*, Math. Models Methods Appl. Sci., 23 (2013), pp. 1979–2003.

[6] L. Beirão da Veiga, A. Buffa, G. Sangalli, and R. Vázquez, *Mathematical analysis of variational isogeometric methods*, Acta Numer., 23 (2014), pp. 157–287.

[7] L. Beirão da Veiga, D. Cho, L. F. Pavarino, and S. Scacchi, *BDDC preconditioners for isogeometric analysis*, Math. Models Methods Appl. Sci., 23 (2013), pp. 1099 – 1142.

[8] ——, *Isogeometric Schwarz preconditioners for linear elasticity systems*, Comput. Methods Appl. Mech. Engrg., 253 (2013), pp. 439 – 454.

[9] J. H. Bramble, J. E. Pasciak, J. P. Wang, and J. Xu, *Convergence estimates for multigrid algorithms without regularity assumptions*, Math. Comp., 57 (1991), pp. 23–45.

[10] J. H. Bramble, J. E. Pasciak, and J. Xu, *Parallel multilevel preconditioners*, Math. Comp., 55 (1990), pp. 1–22.

[11] S. C. Brenner and L. R. Scott, *The mathematical theory of finite element methods*, vol. 15 of Texts in Applied Mathematics, Springer-Verlag, New York, 1994.

[12] A. Bressan, A. Buffa, and G. Sangalli, *Characterization of analysis-suitable T-splines*, Comput. Aided Geom. Design, 39 (2015), pp. 17 – 49.

[13] A. Buffa and C. Giannelli, *Adaptive isogeometric methods with hierarchical splines: Error estimator and convergence*, Math. Models Methods Appl. Sci., 26 (2016), pp. 1–25.

[14] A. Buffa, H. Harbrecht, A. Kunoth, and G. Sangalli, *BPX-preconditioning for isogeometric analysis*, Comput. Methods Appl. Mech. Engrg., 265 (2013), pp. 63 – 70.

[15] L. Chen, R. H. Nochetto, and J. Xu, *Optimal multilevel methods for graded bisection grids*, Numer. Math., 120 (2012), pp. 1–34.

[16] J. A. Cottrell, T. J. R. Hughes, and Y. Bazilevs, *Isogeometric Analysis: toward integration of CAD and FEA*, John Wiley & Sons, 2009.

[17] C. de Boor, *A practical guide to splines*, vol. 27 of Applied Mathematical Sciences, Springer-Verlag, New York, revised ed., 2001.

[18] C. de Falco, A. Reali, and R. Vázquez, *GeoPDEs: a research tool for Isogeometric Analysis of PDEs*, Adv. Engrg. Softw., 42 (2011), pp. 1020–1034.

[19] T. Dokken, T. Lyche, and K. F. Pettersen, *Polynomial splines over locally refined box-partitions*, Comput. Aided Geom. Design, 30 (2013), pp. 331–356.

[20] M. Donatelli, C. Garoni, C. Manni, S. Serra-Capizzano, and H. Speleers, *Robust and optimal multi-iterative techniques for IgA Galerkin linear systems*, Comput. Methods Appl. Mech. Engrg., 284 (2015), pp. 230–264.

[21] ——, *Symbol-Based Multigrid Methods for Galerkin B-Spline Isogeometric Analysis*, SIAM J. Numer. Anal., 55 (2017), pp. 31–62.

[22] M. Dörfel, B. Jüttler, and B. Simeon, *Adaptive isogeometric analysis by local h-refinement with T-splines*, Comput. Methods Appl. Mech. Engrg., 199 (2010), pp. 264 – 275.

[23] K. Gahalaut, J. Kraus, and S. Tomar, *Multigrid methods for isogeometric discretization*, Comput. Methods Appl. Mech. Engrg., 253 (2013), pp. 413 – 425.

[24] C. Hofreither, S. Takacs, and W. Zulehner, *A robust multigrid method for Isogeometric Analysis in two dimensions using boundary correction*, Comput. Methods Appl. Mech. Engrg., (2016), pp. –. In press.

[25] C. Hofreither and W. Zulehner, *Mass smoothers in geometric multigrid for isogeometric analysis*, in Curves and surfaces, vol. 9213 of Lecture Notes in Comput. Sci., Springer, Cham, 2015, pp. 272–279.

[26] ——, *Spectral analysis of geometric multigrid methods for isogeometric analysis*, in Numerical methods and applications, vol. 8962 of Lecture Notes in Comput. Sci., Springer, Cham, 2015, pp. 123–129.

[27] T. J. R. Hughes, J. A. Cottrell, and Y. Bazilevs, *Isogeometric analysis: CAD, finite elements, NURBS, exact geometry and mesh refinement*, Comput. Methods Appl. Mech. Engrg., 194 (2005), pp. 4135–4195.

[28] K. A. Johannessen, T. Kvamsdal, and T. Dokken, *Isogeometric analysis using LR B-splines*, Comput. Methods Appl. Mech. Engrg., 269 (2014), pp. 471 – 514.

[29] S. K. Kleiss, C. Pechstein, B. Jüttler, and S. Tomar, *IETI—isogeometric tearing and interconnecting*, Comput. Methods Appl. Mech. Engrg., 247/248 (2012), pp. 201–215.

[30] X. Li and M. A. Scott, *Analysis-suitable T-splines: Characterization, refineability, and approximation*, Math. Models Methods Appl. Sci., 24 (2014), pp. 1141–1164.

[31] X. Li, J. Zheng, T. Sederberg, T. Hughes, and M. Scott, *On linear independence of T-spline blending functions*, Comput. Aided Geom. Design, 29 (2012), pp. 63 – 76.

[32] P. Morgenstern and D. Peterseim, *Analysis-suitable adaptive T-mesh refinement with linear complexity*, Comput. Aided Geom. Design, 34 (2015), pp. 50–66.

[33] L. F. Pavarino and S. Scacchi, *Isogeometric block FETI-DP preconditioners for the Stokes and mixed linear elasticity systems*, Comput. Methods Appl. Mech. Engrg., 310 (2016), pp. 694–710.

[34] L. L. Schumaker, *Spline functions: basic theory*, Cambridge Mathematical Library, Cambridge University Press, Cambridge, third ed., 2007.

[35] M. Scott, X. Li, T. Sederberg, and T. J. R. Hughes, *Local refinement of analysis-suitable T-splines*, Comput. Methods Appl. Mech. Engrg., 213 - 216 (2012), pp. 206 – 222.

[36] T. Sederberg, J. Zheng, A. Bakenov, and A. Nasri, *T-splines and T-NURCCSs*, ACM Trans. Graph., 22 (2003), pp. 477–484.

[37] R. Vázquez, *A new design for the implementation of isogeometric analysis in Octave and Matlab: GeoPDEs 3.0*, Comput. Math. Appl., 72 (2016), pp. 523 – 554.

[38] A.-V. Vuong, C. Giannelli, B. Jüttler, and B. Simeon, *A hierarchical approach to adaptive local refinement in isogeometric analysis*, Comput. Methods Appl. Mech. Engrg., 200 (2011), pp. 3554–3567.

[39] X. Wei, Y. Zhang, L. Liu, and T. J. Hughes, *Truncated T-splines: Fundamentals and methods*, Comput. Methods Appl. Mech. Engrg., (2016), pp. –. In press.

[40] J. Xu, *An introduction to multigrid convergence theory*, in Iterative methods in scientific computing (Hong Kong, 1995), Springer, Singapore, 1997, pp. 169–241.

[41] J. Xu, L. Chen, and R. H. Nochetto, *Optimal multilevel methods for H(grad), H(curl), and H(div) systems on graded and unstructured grids*, in Multiscale, nonlinear and adaptive approximation, Springer, Berlin, 2009, pp. 599–659.

Recent titles from the IMATI-REPORT Series:

2016

16-01: *Optimal strategies for a time-dependent harvesting problem*, G.M. Coclite, M. Garavello, L.V. Spinolo.

16-02: *A new design for the implementation of isogeometric analysis in Octave and Matlab: GeoPDEs 3.0,* R. Vázquez.

16-03: *Defect detection in nanostructures*, D. Carrera, F. Manganini, G. Boracchi, E. Lanzarone.

16-04: *A study of the state of the art of process planning for additive manufacturing*, M. Livesu, M. Attene, M. Spagnuolo, B. Falcidieno.

16-05: *Calcolo di descrittori ibridi geometria-colore per l'analisi di similarità di forme 3D,* A. Raffo, S. Biasotti.

16-06: *An appointment scheduling framework to balance the production of blood bags from donation*, S. Baş, G. Carello, E. Lanzarone, S. Yalçındağ.

16-07: *From lesson learned to the refactoring of the DRIHM science gateway for hydro-meteorological research,* D. D'Agostino, E. Danovaro, A. Clematis, L. Roverelli, G. Zereik, A. Galizia.

16-08: *Algorithms for the implementation of adaptive isogeometric methods using hierarchical splines*, E.M. Garau, R. Vázquez.

16-09: *Feature curve identification in archaeological fragments using an extension of the Hough transform,* M.L. Torrente, S. Biasotti, B. Falcidieno.

16-10: *Comparing methods for the approximation of rainfall fields in environmental applications,* G. Patané, A. Cerri, V. Skytt, S. Pittaluga, S. Biasotti, D. Sobrero, T. Dokken, M. Spagnuolo.

16-11: *Persistence-based tracking of rainfall field maxima*, S. Biasotti, A.Cerri, S. Pittaluga, D. Sobrero, M. Spagnuolo.

16-12: *Studio e sviluppo di componenti semantiche riusabili per la progettazione di serious game. Applicazioni all'area edutainment,* A. Repetto, C.E. Catalano.

16-13: *Optimal-order isogeometric collocation at Galerkin superconvergent points,* M. Montardini, G. Sangalli, L. Tamellini.

16-14: *Identification of patterns of repeated parts in solid objects*, L. Chiang, F. Giannini, M. Monti.

16-15: *Identification of patterns of repeated parts in solid objects Part II*, L. Chiang, F. Giannini, M. Monti.

16-16: *A machine learning based framework for mapping aesthetic properties to 3D free form shapes*, A. Petrov, J-P. Pernot, F. Giannini, B. Falcidieno, P. Véron

16-17: *Conceptual design of shapes in Virtual Environments through the re-use of heterogeneous data*, Z. Li, F. Giannini, J-P. Pernot, P. Véron, B. Falcidieno

2017

17-01: *BPX preconditioners for isogeometric analysis using analysis-suitable T-splines,* D. Cho, R. Vázquez.